

\mathcal{CP} structure of the top-quark Yukawa interaction: NLO QCD corrections and off-shell effects

Jonathan Hermann, Daniel Stremmer and Malgorzata Worek

*Institute for Theoretical Particle Physics and Cosmology, RWTH Aachen University,
D-52056 Aachen, Germany*

E-mail: jonathan.hermann@rwth-aachen.de, daniel.stremmer@rwth-aachen.de,
worek@physik.rwth-aachen.de

ABSTRACT: Since its discovery at the Large Hadron Collider in 2012 the Higgs boson has arguably become the most famous of the Standard Model particles and many measurements have been performed in order to assess its properties. Among others, these include measurements of the Higgs boson's \mathcal{CP} state which is predicted to be \mathcal{CP} -even. Even though a pure \mathcal{CP} -odd state has been ruled out, a possible admixture of a \mathcal{CP} -odd Higgs state has yet to be excluded. In this work we present predictions for the associated production of a leptonically decaying top quark pair and a stable Higgs boson $pp \rightarrow e^+ \nu_e \mu^- \bar{\nu}_\mu b \bar{b} H$ with possible mixing between \mathcal{CP} -even and \mathcal{CP} -odd states at NLO in QCD for the LHC with $\sqrt{s} = 13$ TeV. Finite top-quark and gauge boson width effects as well as all double-, single- and non-resonant Feynman diagrams including their interference effects are taken into account. We compare the behaviour of the \mathcal{CP} -even, -odd and -mixed scenarios for the integrated fiducial cross-sections as well as several key differential distributions. In addition, we show that both NLO corrections and off-shell effects play an important role even at the level of integrated fiducial cross-sections and that these are further enhanced in differential distributions. Even though we focus here on the Standard Model Higgs boson, the calculations could be straightforwardly applied to models that have an extended Higgs-boson sector and predict the existence of \mathcal{CP} -odd Higgs-like particles, such as the two-Higgs-doublet model.

KEYWORDS: Higher Order Perturbative Calculations, Top Quark, Higgs Production, Higgs Properties

TTK-22-19, P3H-22-054

Contents

1	Introduction	1
2	Description of the calculation and Higgs parametrisation	4
3	LHC setup	6
4	Integrated fiducial cross-sections	7
5	Differential fiducial cross-sections	12
6	Summary	25

1 Introduction

The discovery of the Higgs boson with a mass of 125 GeV by the ATLAS and CMS collaborations in 2012 [1, 2] has launched an extensive research program to establish the true origin of this particle and probe all its properties. Determination of its couplings to the Standard Model (SM) particles and verification of its quantum numbers are among the most important tasks for current and future runs of the LHC and, in fact, for any future collider. Accurate measurements of the Higgs boson’s properties are critical for validating the SM or potentially discovering new physical effects by detecting deviations from the SM predictions. The \mathcal{CP} nature of the Higgs boson has been extensively studied at the LHC. As a matter of fact, LHC measurements have already ruled out the hypothesis of the pure \mathcal{CP} -odd Higgs boson [3, 4]. However, only rather weak constraints exist on a possible admixture between a \mathcal{CP} -even and \mathcal{CP} -odd component. Moreover, most existing experimental analyses concentrate on the coupling of the Higgs boson to two massive gauge bosons HVV , where $V = Z, W$. In particular, both ATLAS and CMS have investigated Higgs boson production via vector-boson fusion as well as the following decays $H \rightarrow ZZ^* \rightarrow 4\ell$ and $H \rightarrow WW^* \rightarrow 2\ell 2\nu$, see e.g. Refs. [5–10]. It seems that so far the properties of the discovered Higgs boson agree with the predictions of the SM [11–13]. It remains an intriguing possibility, however, that the observed Higgs boson might just be one member of an extended Higgs boson sector. A very good motivation for such a beyond the SM Higgs boson sector is the fact that it allows for a new source of \mathcal{CP} violation. The latter is required to explain the matter–antimatter asymmetry problem in the observed universe [14]. Several competing hypotheses exist to explain the imbalance of matter and antimatter that resulted in baryogenesis. As of yet, there is no consensus theory explaining this phenomenon. However, it is clear that \mathcal{CP} violation in the SM is insufficient for this purpose [15]. Thus, we are forced to look elsewhere and, in particular, beyond the well-known SM. Among the simplest Higgs boson extensions are the Two-Higgs-Doublet models (2HDMs) where the SM is extended by one extra Higgs boson doublet with the same quantum numbers as the SM one [16–19]. These 2HDMs, both in their \mathcal{CP} -conserving and \mathcal{CP} -violating versions, are usually used as benchmark models to search for new scalars at the LHC. The 2HDM has four extra degrees of freedom with two extra neutral scalars and two charged scalars. In the \mathcal{CP} -conserving version of a generic 2HDM the two neutral states are \mathcal{CP} -even (often denoted as h, H) and one is \mathcal{CP} -odd (often

denoted as A). Moreover, in this case there are no tree-level couplings between the pseudoscalar Higgs boson and vector bosons as the bosonic sectors of most 2HDM extensions conserve parity. Thus, AZZ and AWW couplings must be induced through fermion loops. The branching ratios for $A \rightarrow ZZ$ and $A \rightarrow WW$ decays are usually expected to be small, however, Higgs-fermion couplings can be enhanced by large fermion masses and other model parameters. On the other hand, in the \mathcal{CP} -violating version of a generic 2HDM, the three neutral states are a mixture of \mathcal{CP} -even and \mathcal{CP} -odd states. In addition, one of the three states is identified as the 125 GeV Higgs boson and all of them have non-zero HZZ and HWW type interactions. Consequently, one must also concentrate on investigating the couplings of the observed Higgs boson to the SM fermions. Such studies are of the utmost importance to settle the question of the true nature of this recently discovered Higgs boson. Of all the SM fermions, the top quark plays a special role due to its large mass of $m_t = 172.5$ GeV. The top-quark Yukawa coupling (Y_t) is the only coupling with the magnitude of the order of one in the SM. Any hint of the \mathcal{CP} -odd or \mathcal{CP} -mixed component would first manifest itself in the connection with the top quarks, for example in the $t\bar{t}H$ production process. Such a modified coupling would be a direct indication of the presence of new physics. Furthermore, it would impact not only integrated cross-sections but also various differential cross-section distributions, see e.g. [20–23].

Indirect measurements of the Yukawa coupling between the Higgs boson and the top quark have been carried out at the LHC using the gluon fusion process, very often with $H \rightarrow \gamma\gamma$ decays [24–27]. In such a case, the production and, depending on the final state, the decay occur via virtual loops [24–27]. Therefore, these measurements have been largely based on the assumption that no unknown particles are allowed in these loops. A direct test of the Y_t coupling can be performed through the production of the Higgs boson in association with a top quark pair. In 2018 this process was observed by the ATLAS and CMS collaborations [28, 29]. Recently, ATLAS and CMS have reported first experimental Higgs-top \mathcal{CP} studies, exploring the $t\bar{t}H$ process with various Higgs boson decay channels [30–32]. Even though the measurements favor the SM Higgs-top coupling, the \mathcal{CP} -violating coupling has not yet been excluded. Using the Higgs boson decays to two photons, the ATLAS collaboration has been able to exclude the purely \mathcal{CP} -odd hypothesis with 3.9 standard deviations and establish a 95% C.L. exclusion limit for the mixing angle of 43° . On the other hand, the CMS collaboration has performed the first measurement of the \mathcal{CP} mixing angle for the τ lepton Yukawa coupling [33] which has been found to be $4^\circ \pm 17^\circ$. This has allowed them to set an exclusion limit on the mixing angle of 36° . Of course for current and future comparisons with increasingly accurate experimental measurements by ATLAS and CMS, equally precise theoretical predictions must also be provided.

The effective Lagrangian for the spin $\mathcal{J} = 0$ state can be written down using the so-called Higgs characterisation model [34]. In this parametrisation, the SM case, i.e. the \mathcal{CP} -even state that is invariant under charge-parity (\mathcal{CP}) inversion and described by $\mathcal{J}^{\mathcal{CP}} = 0^{++}$, can easily be recovered. Furthermore, a \mathcal{CP} -odd state as described by $\mathcal{J}^{\mathcal{CP}} = 0^{+-}$, which is typical for a generic 2HDM, is included. In addition, \mathcal{CP} mixing between the \mathcal{CP} -even and \mathcal{CP} -odd state is allowed and it is parameterised in terms of the mixing angle $\alpha_{\mathcal{CP}}$. Finally, within this framework the \mathcal{CP} -odd, \mathcal{CP} -even and \mathcal{CP} -mixed states can all couple to SM particles. In practice, the effective Lagrangian that describes the top Yukawa coupling can be written as a superposition of a \mathcal{CP} -even and a \mathcal{CP} -odd phase. Any deviation from the SM value for the coupling would indicate \mathcal{CP} violation in the top-Higgs sector and could be immediately translated into new physics effects beyond the SM.

The Higgs characterisation model has been studied extensively in the literature. These studies include, among other processes, the Higgs boson production in association with top quarks, see e.g. Refs. [35–40]. The impact of higher-order corrections on \mathcal{CP} -sensitive observables has been investigated

e.g. in Refs. [41–48]. Specifically, $pp \rightarrow t\bar{t}H$ production, the combined t -channel $tH + \bar{t}H$ production process and tWH have been studied including parton shower effects. For all three processes next-to-leading-order (NLO) QCD corrections have only been taken into account for the production stage while top-quark decays have been treated using parton shower approximations. In some cases spin-correlated LO top-quark decays have been included as well. In practise, however, such simulations are always based on the on-shell top-quark approximation. Moreover, for the computation of NLO QCD corrections to the tWH process the isolation of the $t\bar{t}H$ process and elimination of its double resonant contributions is required. In order to achieve this, the authors have used subtractions that are fully local in the phase space. Specifically, they have applied the two main schemes that are present in the literature and are known under the name of diagram removal and diagram subtraction [49]. However, the only way to perform theoretically consistent simulations that comprise both $t\bar{t}H$ and $tW(b)H$ is to compute the $pp \rightarrow W^+bW^-\bar{b}H$ process using a complex top-quark mass. We point out here that the tWH contribution in the final state with one b -jet can be obtained with massive bottom quarks using the four-flavour scheme (see e.g. [50] for a simpler case of $t\bar{t}$ and tW). Instead, for $tWbH$ in the final state with two b -jets, massless bottom quarks and the five flavour-scheme can be employed. A simulation of the $pp \rightarrow W^+bW^-\bar{b}H$ process would include all contributions that are, on the one hand, gauge invariant and, on the other hand, include interference and finite top-quark width effects. It would also contain contributions from the amplitude without any resonant top-quark propagator and, in turn, interference effects between single-top and single-antitop contributions. The latter are absent in $tWbH$ simulations. A particular final state that we are interested in can be enhanced and probed by means of kinematic cuts, closely following what is being done in the ATLAS and CMS experiments. We note that such full NLO QCD predictions for the $t\bar{t}H$ process with leptonic top-quark decays exist but only for the \mathcal{CP} -even case [51, 52]. Later also electroweak corrections have been calculated for this process [53]. Very recently even various Higgs boson decays have been added albeit in the narrow-width-approximation (NWA) [52]. Taking into account how crucial the measurements of the top-quark Yukawa coupling are, it is of utmost importance to provide the full NLO QCD calculation for the $t\bar{t}H$ process allowing beyond the SM top-Higgs couplings and taking into account all effects whilst consistently avoiding any approximations.

The purpose of the article is, therefore, manifold. Firstly, we provide state-of-the-art NLO QCD predictions for the $pp \rightarrow t\bar{t}H$ process in the di-lepton top-quark decay channel with an extended top-Higgs Yukawa coupling within the Higgs characterisation framework. Specifically, we calculate NLO QCD corrections to the $e^+\nu_e\mu^-\bar{\nu}_\mu b\bar{b}H$ final state, consistently taking into account double-, single and non-resonant top-quark contributions together with all interference effects. Moreover, in the computation off-shell, top quarks are treated in the complex mass scheme with a physical top-quark width Γ_t . Similarly, non-resonant and off-shell effects due to the finite W boson width are also incorporated in the calculation. Schematically, our calculations for the $e^+\nu_e\mu^-\bar{\nu}_\mu b\bar{b}H$ matrix element squared can be written down as $|\mathcal{M}_{t\bar{t}H}|^2 = |\mathcal{M}_{2tH} + \mathcal{M}_{1tH} + \mathcal{M}_{1\bar{t}H} + \mathcal{M}_{0tH}|^2$. Secondly, we investigate the sensitivity of the $t\bar{t}H$ process to beyond the SM physics in the Higgs boson sector and identify observables that are particularly useful in distinguishing the three different Higgs boson \mathcal{CP} states. Thirdly, we assess the impact of full off-shell effects on the $t\bar{t}H$ process with the extended top-Higgs coupling both at the integrated and differential fiducial cross-section level. To perform such a study, a second computation based on the NWA is carried out for the $pp \rightarrow t\bar{t}H$ process. In this case the $e^+\nu_e\mu^-\bar{\nu}_\mu b\bar{b}H$ final state is generated in the $pp \rightarrow t\bar{t}H \rightarrow W^+bW^-\bar{b}H \rightarrow e^+\nu_e\mu^-\bar{\nu}_\mu b\bar{b}H$ decay chain where the top quarks and W gauge bosons are always kept on-shell. On the one hand, we compare our results from the full off-shell calculation to the predictions based on the full NWA. In that case

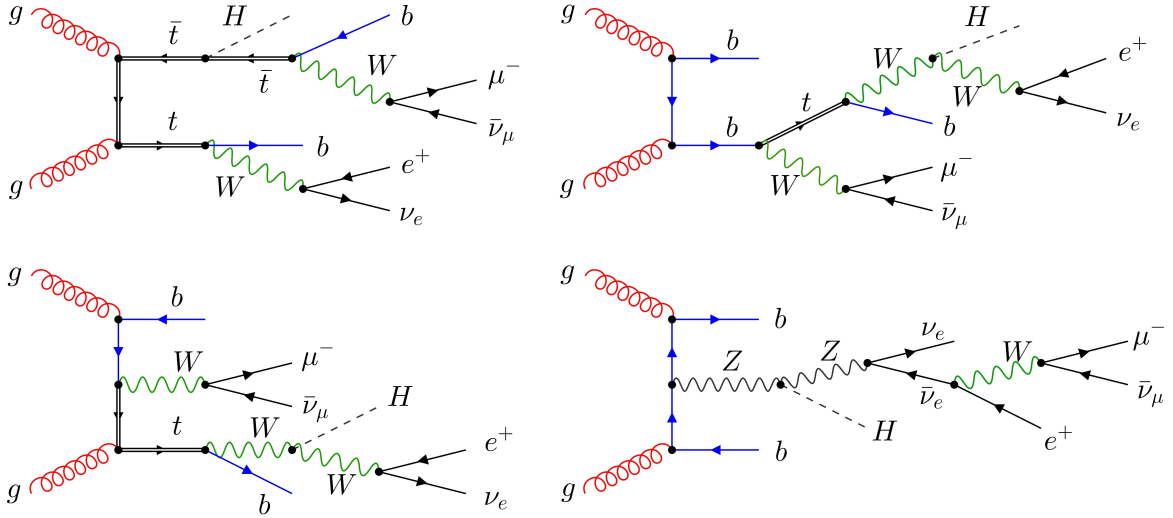


Figure 1: Representative LO Feynman diagrams for the $pp \rightarrow e^+ \nu_e \mu^- \bar{\nu}_\mu b \bar{b} H$ process involving two (top left), only one (top right and bottom left) or no (bottom right) top-quark resonances. The Feynman diagrams were created with the help of the FEYNGAME [54] program.

NLO QCD corrections are calculated both to the production stage and the top-quark decays. On the other hand, we also provide NLO QCD predictions in the NWA but with leading order (LO) top-quark decays (abbreviated as $\text{NWA}_{\text{LOdec}}$). By employing the NWA and $\text{NWA}_{\text{LOdec}}$ results, we are able to estimate the effects of NLO QCD corrections to the top-quark decays.

The paper is organised as follows. In Section 2 we summarise the framework of our calculation. The theoretical setup for LO and NLO QCD results is given in Section 3. Results for the integrated fiducial cross-sections for the SM (\mathcal{CP} -even), \mathcal{CP} -mixed and \mathcal{CP} -odd Higgs boson are presented in Section 4. In Section 5 predictions for differential fiducial cross-sections are given and we investigate how the different \mathcal{CP} configurations are affected by the higher-order effects in various phase-space regions. Additionally, we present observables that can be used to distinguish the \mathcal{CP} states. Finally, in Section 5 we study the impact of off-shell effects on differential fiducial cross sections and examine the size of NLO QCD corrections to top-quark decays at the differential level. We summarise the results and outline our conclusions in Section 6.

2 Description of the calculation and Higgs parametrisation

In this work we consider the production of a stable \mathcal{CP} -even, \mathcal{CP} -odd and \mathcal{CP} -mixed Higgs boson in association with a leptonically decaying top-quark pair at order $\mathcal{O}(\alpha_s^3 \alpha^5)$ in perturbation theory. Specifically, we study the process $pp \rightarrow e^+ \nu_e \mu^- \bar{\nu}_\mu b \bar{b} H + X$, i.e. we calculate NLO QCD corrections to the LO process $pp \rightarrow e^+ \nu_e \mu^- \bar{\nu}_\mu b \bar{b} H$ which is of order $\mathcal{O}(\alpha_s^2 \alpha^5)$. Following the Higgs characterisation framework [34], we allow for a possible admixture of a \mathcal{CP} -odd Higgs state and extend the top Yukawa interaction according to

$$\mathcal{L}_{t\bar{t}H} = -\bar{\psi}_t \frac{Y_t}{\sqrt{2}} (\kappa_{H\bar{t}t} \cos(\alpha_{\mathcal{CP}}) + i\kappa_{A\bar{t}t} \sin(\alpha_{\mathcal{CP}})\gamma_5) \psi_t H, \quad (2.1)$$

where ψ_t and H are the top and Higgs fields, respectively, whereas α_{CP} is the \mathcal{CP} -mixing angle. Furthermore, $Y_t = \sqrt{2}m_t/v$ is the top quark Yukawa coupling with the Higgs vacuum expectation value $v \approx 246$ GeV and the top quark mass m_t . In this parametrisation:

- $\alpha_{CP} = 0$ corresponds to the \mathcal{CP} -even case,
- $\alpha_{CP} = \pi/2$ corresponds to the \mathcal{CP} -odd case,
- $\alpha_{CP} = \pi/4$ corresponds to the \mathcal{CP} -mixed case.

In practice, a \mathcal{CP} -mixed scenario could be realised by choosing any value of α_{CP} from the range $\alpha_{CP} \in (0, \pi/2)$ but we focus here on the $\alpha_{CP} = \pi/4$ case for which $\cos(\alpha_{CP}) = \sin(\alpha_{CP})$. Different choices for the real-valued couplings $\kappa_{Ht\bar{t}}$ and $\kappa_{At\bar{t}}$ will be discussed in Section 4. In addition to changing the Yukawa interaction, we also introduce an additional parameter κ_{HVV} in the HVV ($V = W^\pm, Z$) interaction term

$$\mathcal{L}_{HVV} = \kappa_{HVV} \left(\frac{1}{2} g_{HZZ} Z_\mu Z^\mu + g_{HWW} W_\mu^+ W^{-\mu} \right) H, \quad (2.2)$$

where $g_{HZZ} = 2m_Z^2/v$ and $g_{HWW} = 2m_W^2/v$ are the HVV couplings with $m_{Z,W}$ being the masses of the electroweak (EW) gauge bosons. We do not take into account higher dimensional HVV couplings and neglect any contribution from loop-induced couplings of the Higgs boson to gluons or photons. The above described HVV couplings are only of importance in full off-shell calculations such as the one presented here since on-shell top quarks are not heavy enough to produce both a Higgs and a W boson.

In order to incorporate full off-shell effects, we consistently take into account all Feynman diagrams with the $e^+ \nu_e \mu^- \bar{\nu}_\mu b\bar{b} H$ final state at order $\mathcal{O}(\alpha_s^2 \alpha^5)$ (for the LO computation) and interference effects, irrespective of whether a $t\bar{t}$ pair actually occurs as an intermediate state. The same applies to the W bosons appearing in the calculation. Examples for such diagrams with two, only one or no top-quark resonances, to which we will be referring as double-, single- and non-resonant contributions in the following, are depicted in Figure 1. Assuming a diagonal Cabibbo-Kobayashi-Maskawa (CKM) matrix and using the 5-flavor scheme, i.e. setting both the mass and the Yukawa coupling of the bottom quark to zero, we obtain 174 diagrams for the $g\bar{g}$ and 76 for the $q\bar{q}$ initial state at LO where $q \in \{u, d, c, s\}$. On the other hand, $b\bar{b}$ initial states are neglected as they are at the per-mille level [52] and thus well within NLO scale uncertainties. The numbers of diagrams are independent of the \mathcal{CP} -structure of the Higgs boson as long as $\kappa_{HVV}, \kappa_{At\bar{t}}, \kappa_{Ht\bar{t}} \neq 0$. To include Breit-Wigner propagators for the top quark and gauge bosons in a gauge invariant way, we use the complex-mass scheme [55–58]. In addition to the full off-shell case we also provide results in the NWA, i.e. the limit in which the unstable intermediate top quarks and W gauge bosons are put on-shell. As only double-resonant diagrams (see e.g. top-left diagram in Figure 1) are included when employing the NWA, the numbers of considered diagrams for the $g\bar{g}$ and $q\bar{q}$ initial states are reduced to 8 and 2, respectively, at LO.

All of the results presented in this work were obtained using the HELAC-NLO [59, 60] MC program which consists of HELAC-DIPOLES [61] and HELAC-1LOOP [62]. Amplitudes are constructed in a recursive manner based on recursive Dyson-Schwinger equations [63–65] and the phase-space integration is performed with the help of PARNI [66] and KALEU [67]. NLO corrections to the Born level process can be divided into virtual and real corrections which are computed in HELAC-1LOOP and HELAC-DIPOLES, respectively. Note that from the point of view of QCD corrections, this process is essentially identical to $t\bar{t}\gamma$, $t\bar{t}W^\pm$ or $t\bar{t}Z$ production as presented in Refs. [68–70]. For the virtual corrections we use the CUTTOOLS [71] implementation of the OPP reduction [72] in order to reduce

the occurring one loop amplitudes to scalar integrals at the integrand level. The resulting scalar integrals are then evaluated using ONELOOP [73]. The real corrections receive contributions from $2 \rightarrow 8$ partonic processes. In our case we need to consider the following subprocesses:

$$\begin{aligned}
gg &\rightarrow e^+ \nu_e \mu^- \bar{\nu}_\mu b\bar{b} Hg \\
q\bar{q} &\rightarrow e^+ \nu_e \mu^- \bar{\nu}_\mu b\bar{b} Hg \\
gq &\rightarrow e^+ \nu_e \mu^- \bar{\nu}_\mu b\bar{b} Hq \\
g\bar{q} &\rightarrow e^+ \nu_e \mu^- \bar{\nu}_\mu b\bar{b} H\bar{q}
\end{aligned}
\tag{2.3}$$

Their respective contributions are computed using HELAC-DIPOLES. It implements two independent subtraction schemes, the Catani-Seymour dipole formalism [74, 75] and the Nagy-Soper subtraction scheme [76]. We use the Nagy-Soper scheme for the full off-shell calculations while those done in the NWA are performed in the Catani-Seymour formalism and its extension to top-quark decays [60, 77].

Our full off-shell results are stored as (partially) unweighted events [78] in (modified) Les Houches Event Files (LHEFs) [79] and ROOT Ntuples [80]. This allows us to re-weight our results in order to efficiently accommodate different parton distribution functions (PDFs) as well as renormalisation and factorisation scale settings.

The implementation of the modified HVV and $Ht\bar{t}$ interactions in HELAC-NLO according to equations (2.1) and (2.2) have been cross-checked with MADGRAPH_AMC@NLO [81] and MADLOOP [82]. Furthermore, various tests have been performed within the HELAC-NLO code. Specifically, we have compared the LO full off-shell squared amplitudes for $gg \rightarrow e^+ \nu_e \mu^- \bar{\nu}_\mu b\bar{b} H$ and $u\bar{u} \rightarrow e^+ \nu_e \mu^- \bar{\nu}_\mu b\bar{b} H$ with MADGRAPH_AMC@NLO for a few random phase-space points. The latter have been generated with the help of the RAMBO [83] MC phase-space generator. In addition, we have checked the finite parts along with the coefficients of the poles in ϵ , i.e. $1/\epsilon$ and $1/\epsilon^2$, of the virtual amplitudes for stable $t\bar{t}H$ production for gg and $u\bar{u}$ initial states for all three \mathcal{CP} states. For the real corrections we have ensured that the poles in ϵ occurring in the \mathbf{I} -operator and those appearing in the virtual part cancel. Finally, we have confirmed that the real emission part is independent from any phase-space restriction imposed by the unphysical α_{max} parameter [84–87].

3 LHC setup

We consider the \mathcal{CP} -even, \mathcal{CP} -odd and \mathcal{CP} -mixed Higgs production in association with top quarks at the LHC with $\sqrt{s} = 13$ TeV and calculate higher-order corrections to the $e^+ \nu_e \mu^- \bar{\nu}_\mu b\bar{b} H$ final state at $\mathcal{O}(\alpha_s^3 \alpha^5)$. We work in the 5-flavour scheme ($N_f = 5$) and neglect the contribution from bottom quarks in the initial state. The LHAPDF interface [88] is used to provide an access to parton density functions and we employ the NNPDF31-nlo-as-0118 PDF set [89] with $\alpha_s(m_Z) = 0.118$ at LO and NLO in QCD. The running of the strong coupling constant is performed with two-loop accuracy. The G_μ -scheme is used for the electroweak input parameters and we adopt the same values as in Ref. [70]. Thus, the electromagnetic coupling constant α is given by

$$\alpha = \frac{\sqrt{2}}{\pi} G_\mu m_W^2 \left(1 - \frac{m_W^2}{m_Z^2} \right), \quad G_\mu = 1.166378 \cdot 10^{-5} \text{ GeV}^{-2}. \tag{3.1}$$

We use the following masses and widths

$$\begin{aligned}
m_t &= 172.5 \text{ GeV}, & m_H &= 125 \text{ GeV}, \\
m_W &= 80.385 \text{ GeV}, & \Gamma_W &= 2.09767 \text{ GeV}, \\
m_Z &= 91.1876 \text{ GeV}, & \Gamma_Z &= 2.50775 \text{ GeV},
\end{aligned}
\tag{3.2}$$

and neglect the masses of all other particles. From these input parameters we calculate the top-quark width according to the formulae derived in Refs. [58, 90]. For the values provided above, the LO and NLO top-quark widths are given by

$$\Gamma_t^{\text{LO}} = 1.45759 \text{ GeV}, \quad \Gamma_t^{\text{NLO}} = 1.33247 \text{ GeV} \quad (3.3)$$

in the full off-shell case and by

$$\Gamma_{t,\text{NWA}}^{\text{LO}} = 1.48063 \text{ GeV}, \quad \Gamma_{t,\text{NWA}}^{\text{NLO}} = 1.35355 \text{ GeV} \quad (3.4)$$

in the NWA. The top-quark width is treated as a fixed parameter and we use $\alpha_s(\mu_R = m_t)$ when calculating Γ_t^{NLO} . Since the Higgs boson is stable, its width is set to $\Gamma_H = 0$. IR-safety is ensured by the *anti- k_T* jet algorithm [91] which is used to cluster final state partons with pseudo-rapidity $|\eta| < 5$ into jets with the jet-resolution parameter $R = 0.4$. We require exactly two charged leptons, two b -jets and one stable Higgs boson. All final states have to fulfil the following experimental cuts

$$\begin{aligned} p_{T,\ell} &> 25 \text{ GeV}, & p_{T,b} &> 25 \text{ GeV}, \\ |y_\ell| &< 2.5, & |y_b| &< 2.5, \end{aligned} \quad (3.5)$$

where $\ell = \mu^-, e^+$. No restrictions on the extra light jet and missing transverse momentum, denoted as $p_{T,\text{miss}} = |\vec{p}_{T,\nu_e} + \vec{p}_{T,\bar{\nu}_\mu}|$, are applied. We use a dynamical scale setting $\mu_0 = \mu_R = \mu_F = H_T/2$ as our central scale, where H_T is defined according to

$$H_T = p_{T,b_1} + p_{T,b_2} + p_{T,e^+} + p_{T,\mu^-} + p_{T,\text{miss}} + p_{T,H}, \quad (3.6)$$

where b_1 and b_2 stand for the first and second hardest b -jet in p_T . A detailed discussion and comparison with other scale choices is given for the SM case ($\alpha_{CP} = 0$) in Ref. [52]. In order to estimate the theoretical uncertainties arising from neglected higher-order terms in the perturbative expansion, we use the 7-point scale variation in which the factorisation and renormalisation scales are varied independently in the range

$$\frac{1}{2} \mu_0 \leq \mu_R, \mu_F \leq 2 \mu_0, \quad \frac{1}{2} \leq \frac{\mu_R}{\mu_F} \leq 2. \quad (3.7)$$

This leads to the following seven pairs

$$\left(\frac{\mu_R}{\mu_0}, \frac{\mu_F}{\mu_0} \right) = \left\{ (2, 1), (0.5, 1), (1, 2), (1, 1), (1, 0.5), (2, 2), (0.5, 0.5) \right\}, \quad (3.8)$$

which are taken into account for the error estimation. We do not include PDF uncertainties into the theoretical error estimation, since these are significantly smaller than the scale uncertainties [52], especially for the chosen PDF set.

4 Integrated fiducial cross-sections

In this first part of our analysis we will discuss the results for integrated fiducial cross-sections. The two coupling parameters $\kappa_{H\bar{t}t}$ and $\kappa_{A\bar{t}t}$ appearing in Eq. (2.1) are chosen as follows. We take $\kappa_{H\bar{t}t} = 1$ everywhere to recover the SM results for $\alpha_{CP} = 0$. For $\kappa_{A\bar{t}t}$ we consider two different case, $\kappa_{A\bar{t}t} = 1$ and $\kappa_{A\bar{t}t} = 2/3$. The first choice is simply designed to have the same coupling for both the scalar and pseudoscalar Higgs boson. The second one is motivated by the measurements of Higgs boson production

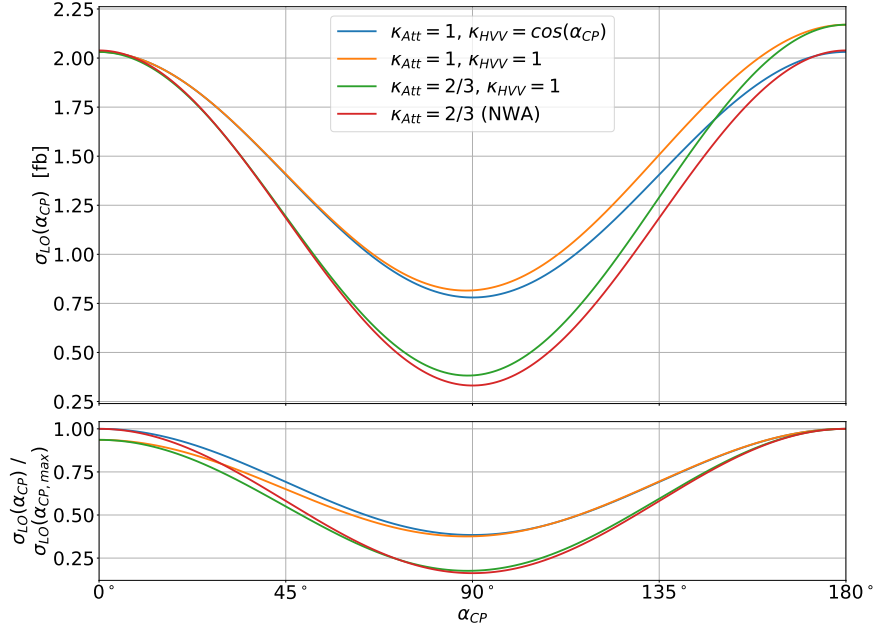


Figure 2: LO integrated fiducial cross-section depending on α_{CP} for the $pp \rightarrow e^+ \nu_e \mu^- \bar{\nu}_\mu b \bar{b} H$ process at the LHC with $\sqrt{s} = 13$ TeV. The red curve indicates the results computed in the NWA for $\kappa_{At\bar{t}} = 2/3$ whereas the blue, orange and green curves correspond to full off-shell results for different choices of the coupling constants. In all cases we have $\kappa_{H\bar{t}t} = 1$. In the lower panel the ratio to $\alpha_{CP, \max}$ is displayed for each plotted case.

in gluon-fusion (GF) process which indicate good agreement with the SM predictions [92, 93]. Assuming that the top-loop induced terms dominate the GF we find

$$\frac{\sigma_{gg \rightarrow H}}{\sigma_{gg \rightarrow H}^{SM}} = \cos^2(\alpha_{CP}) \kappa_{H\bar{t}t}^2 + \sin^2(\alpha_{CP}) \kappa_{At\bar{t}}^2 \frac{g_{A\bar{g}g}^2}{g_{H\bar{g}g}^2} \quad (4.1)$$

for the ratio between the GF in our model and the SM [45, 47]. Here $g_{A\bar{g}g} = \alpha_s / (2\pi v)$ and $g_{H\bar{g}g} = -\alpha_s / (3\pi v)$ are the effective loop-induced gluon-Higgs couplings for a \mathcal{CP} -even and \mathcal{CP} -odd Higgs boson, respectively. Hence, to recover the SM results for any value of α_{CP} one must set $\kappa_{At\bar{t}} = 2/3$ and $\kappa_{H\bar{t}t} = 1$.

For the remaining free parameter κ_{HVV} we also analyse two different cases, specifically $\kappa_{HVV} = \cos(\alpha_{CP})$ and $\kappa_{HVV} = 1$. Note that in the first case κ_{HVV} actually becomes dependent on the mixing angle α_{CP} . This choice is relevant for SM extensions such as the \mathcal{CP} -conserving 2HDM where only \mathcal{CP} -even Higgs-like particles couple to the EW gauge bosons, see e.g. Refs. [18, 94]. Thus, the corresponding couplings receive the same scaling as the scalar Higgs-top coupling. However, when considering a possible non-zero α_{CP} for the SM Higgs boson it is more sensible to choose $\kappa_{HVV} = 1$ in order to recover results from Higgs boson production through vector boson fusion (VBF) which, just as the GF measurements, indicate agreement with the SM [27]. Let us mention that in the NWA, the choice of κ_{HVV} is irrelevant since in this case the Higgs boson can only be radiated off top quarks in the production stage.

In Figure 2 we present the LO integrated fiducial cross-sections depending on the mixing angle α_{CP} for several different combinations of the parameter choices outlined above. The blue, orange and

Table 1: Cross-section coefficients, σ_i , for the splitting of the LO integrated fiducial cross-sections according to Eq. (4.2) for the full off-shell and narrow-width treatments. For the latter the final three coefficients do not contribute as no diagrams with couplings between the Higgs boson and the EW gauge bosons occur in the NWA. The values in brackets indicate the respective Monte Carlo integration error on the last digit.

	Off-shell	NWA
σ_1 [fb]	2.0643(4)	2.0388(2)
σ_2 [fb]	0.7800(1)	0.74583(7)
σ_3 [fb]	-0.0002(8)	-0.0001(3)
σ_4 [fb]	-0.0693(8)	—
σ_5 [fb]	-0.0001(9)	—
σ_6 [fb]	0.0363(9)	—

green curves indicate results for the full off-shell case with different choices for the couplings and the red one describes the NWA with $\kappa_{A\bar{t}\bar{t}} = 2/3$. To create these curves one can make use of the fact that at LO the cross-section can be split into six parts according to

$$\begin{aligned} \sigma(\alpha_{CP}) = & \cos^2(\alpha_{CP}) \kappa_{H\bar{t}\bar{t}}^2 \sigma_1 + \sin^2(\alpha_{CP}) \kappa_{A\bar{t}\bar{t}}^2 \sigma_2 + \cos(\alpha_{CP}) \sin(\alpha_{CP}) \kappa_{H\bar{t}\bar{t}} \kappa_{A\bar{t}\bar{t}} \sigma_3 \\ & + \cos(\alpha_{CP}) \kappa_{H\bar{t}\bar{t}} \kappa_{HV V}(\alpha_{CP}) \sigma_4 + \sin(\alpha_{CP}) \kappa_{A\bar{t}\bar{t}} \kappa_{HV V}(\alpha_{CP}) \sigma_5 + \kappa_{HV V}^2(\alpha_{CP}) \sigma_6, \end{aligned} \quad (4.2)$$

where the σ_i coefficients are independent of the mixing angle, $\kappa_{H\bar{t}\bar{t}}$, $\kappa_{A\bar{t}\bar{t}}$ and $\kappa_{HV V}$. Thus, it is enough to compute six integrated cross-sections with different sets of input parameters $\{\alpha_{CP}, \kappa_{H\bar{t}\bar{t}}, \kappa_{A\bar{t}\bar{t}}, \kappa_{HV V}\}$. From these, the cross-section contributions σ_i in Eq. (4.2) can then be calculated by solving a system of equations. The final results for $\sigma(\alpha_{CP})$ with all required sets of parameters $\{\alpha_{CP}, \kappa_{H\bar{t}\bar{t}}, \kappa_{A\bar{t}\bar{t}}, \kappa_{HV V}\}$ can then easily be assembled from Eq. (4.2). In case of the NWA it is even sufficient to only evaluate the first three contributions as no HVV couplings can occur. Therefore, we have $\sigma_{4,5,6}^{\text{NWA}} = 0$ both at LO and NLO in QCD. The numerical values for the cross-section coefficients σ_i are listed in Table 1. Although there is a non-zero contribution from interference effects between the \mathcal{CP} -odd coupling and the SM contribution at the matrix element level, any hadron collider observable is averaged over charge conjugate processes. As a result, interference effects vanish in typical hadronic (differential) cross-sections when integrated over a \mathcal{CP} -symmetric part of the phase space. This observation still holds for fiducial cross-sections (σ_3, σ_5) when \mathcal{CP} -symmetric selection criteria are applied to all final states, see e.g. Ref. [95].

We note that Eq. (4.2) is also instructive in understanding and interpreting the different behaviours of the curves depicted in Figure 2. First, one should note that the production of pseudoscalar particles in association with top quarks is suppressed compared to scalar ones for masses below ~ 200 GeV if the two couplings $\kappa_{H\bar{t}\bar{t}}$ and $\kappa_{A\bar{t}\bar{t}}$ are equal [96]. This difference can be understood when looking at the

$t \rightarrow t + H/A$ fragmentation functions [97, 98]

$$\begin{aligned} f_{t \rightarrow t+H}(x) &= \frac{\kappa_{Ht\bar{t}}^2}{(4\pi)^2} \left[\frac{4(1-x)}{x} + x \ln \left(\frac{s}{m_t^2} \right) \right], \\ f_{t \rightarrow t+A}(x) &= \frac{\kappa_{At\bar{t}}^2}{(4\pi)^2} \left[x \ln \left(\frac{s}{m_t^2} \right) \right], \end{aligned} \quad (4.3)$$

where x is the momentum fraction that the Higgs boson carries. The scalar fragmentation function has an additional $1/x$ term which enhances the production of soft scalar particles compared to pseudoscalar particles and thus results in a larger integrated fiducial cross-section for a scalar Higgs boson. This can clearly be seen in Figure 2 as all depicted curves have a minimum around $\alpha_{CP} = \pi/2$ which corresponds to the production of a \mathcal{CP} -odd Higgs boson. Reducing $\kappa_{At\bar{t}}$ from 1 to $2/3$ only enhances this effect which is why around its minimum the orange curve ($\kappa_{At\bar{t}} = 1$) is about twice as large as the green one ($\kappa_{At\bar{t}} = 2/3$). For the latter choice of $\kappa_{At\bar{t}}$, the production cross-section of 2.03 fb for a \mathcal{CP} -even Higgs boson is more than five times as large as the 0.38 fb for the \mathcal{CP} -odd case. The mixed case falls almost exactly in the middle with 1.19 fb.

One can also observe that the cross-sections computed in the NWA (red curve) are symmetric with respect to $\alpha_{CP} \rightarrow \pi - \alpha_{CP}$ which is equivalent to changing the sign of the top-quark Yukawa coupling Y_t . As we have $\sigma_{4,5,6}^{\text{NWA}} = 0$ in the NWA, we only need to consider the terms in the first line of Eq. (4.2) in order to understand this phenomenon. For the first two terms the symmetry is inherent in the explicit α_{CP} dependence since $\cos^2(\pi - \alpha_{CP}) = \cos^2(\alpha_{CP})$ and $\sin^2(\pi - \alpha_{CP}) = \sin^2(\alpha_{CP})$. In contrast, for the third term we have $\cos(\pi - \alpha_{CP}) \sin(\pi - \alpha_{CP}) = -\cos(\alpha_{CP}) \sin(\alpha_{CP})$ which means that σ_3 must vanish in order to explain the observed behaviour which is in line with our numerical results in Table 1. From this we can conclude that there is no mixing between the production of \mathcal{CP} -even and \mathcal{CP} -odd Higgs bosons which is known for stable top quarks, see e.g. Ref. [36].

In the full off-shell case we only observe the same symmetry if we set $\kappa_{HVV}(\alpha_{CP}) = \cos(\alpha_{CP})$. With this choice the fourth and sixth term in (4.2) have the same $\cos^2(\alpha_{CP})$ dependence as the first one and the fifth term becomes proportional to $\cos(\alpha_{CP}) \sin(\alpha_{CP})$. As the symmetry of the cross-section under the replacement $\alpha_{CP} \rightarrow \pi - \alpha_{CP}$ is clearly visible in the blue curve of Figure 2, we conclude that both σ_3 and σ_5 must either vanish or cancel, which is again in line with our numerical results. This is broken if we take the other choice for our HVV coupling, $\kappa_{HVV} = 1$, which corresponds to the green and orange curves in Figure 2. In this case the fourth term becomes proportional to just $\cos(\alpha_{CP})$. As the corresponding coefficient is negative, we find that the cross-section for $\alpha_{CP} = \pi$ is actually larger than the one for $\alpha_{CP} = 0$ by about 0.14 fb which translates to an increase of 7%.

Let us also mention that the final term in equation (4.2) becomes independent of α_{CP} when choosing $\kappa_{HVV} = 1$. This means that in this case, the breaking of the symmetry around $\alpha_{CP} = \pi/2$ in the full off-shell case is only a result of the fourth term. This contribution corresponds to the interference between diagrams where the Higgs boson is radiated off a W or Z boson (single- and non-resonant top-quark contributions) with diagrams where the Higgs boson is produced from one of the top quarks (double- and single-resonant top-quark contributions), see Figure 1. As single- and non-resonant Feynman diagrams are absent in the NWA, the dependence on α_{CP} is symmetric in this case. The very different behaviors in the full off-shell treatment and the NWA lead us to conclude that the inclusion of off-shell effects is vital, in particular when considering large mixing angles. Since the discrepancy between the two approaches is mostly driven by the σ_4 term, their difference increases with increasing mixing angle.

This observation also holds at NLO, as can be seen from the integrated fiducial cross-sections listed in Table 2. Here, we compare full off-shell and NWA as well as LO and NLO cross-sections for

Table 2: Comparison of LO and NLO QCD integrated fiducial cross-sections as calculated in the NWA, NWA with LO top-quark decays and full off-shell approach for $\alpha_{CP} = 0, \pi/4$ and $\pi/2$. Also shown are their respective scale uncertainties and Monte Carlo integration errors. All values are given for the $pp \rightarrow e^+ \nu_e \mu^- \bar{\nu}_\mu b\bar{b} H$ process at the LHC with $\sqrt{s} = 13$ TeV.

α_{CP}		Off-shell	NWA	Off-shell effects
0 (SM)	σ_{LO} [fb]	2.0313(2) ^{+0.6275 (31%)} _{-0.4471 (22%)}	2.0388(2) ^{+0.6290 (31%)} _{-0.4483 (22%)}	-0.37%
	σ_{NLO} [fb]	2.466(2) ^{+0.027 (1.1%)} _{-0.112 (4.5%)}	2.475(1) ^{+0.027 (1.1%)} _{-0.113 (4.6%)}	-0.36%
	$\sigma_{NLO_{LOdec}}$ [fb]	—	2.592(1) ^{+0.161 (6.2%)} _{-0.242 (9.3%)}	
	$\mathcal{K} = \sigma_{NLO}/\sigma_{LO}$	1.21	1.21 (LOdec: 1.27)	
$\pi/4$	σ_{LO} [fb]	1.1930(2) ^{+0.3742 (31%)} _{-0.2656 (22%)}	1.1851(1) ^{+0.3707 (31%)} _{-0.2633 (22%)}	0.66%
	σ_{NLO} [fb]	1.465(2) ^{+0.016 (1.1%)} _{-0.071 (4.8%)}	1.452(1) ^{+0.015 (1.0%)} _{-0.069 (4.8%)}	0.89%
	$\sigma_{NLO_{LOdec}}$ [fb]	—	1.517(1) ^{+0.097 (6.4%)} _{-0.144 (9.5%)}	
	$\mathcal{K} = \sigma_{NLO}/\sigma_{LO}$	1.23	1.23 (LOdec: 1.28)	
$\pi/2$	σ_{LO} [fb]	0.38277(6) ^{+0.13123 (34%)} _{-0.09121 (24%)}	0.33148(3) ^{+0.11240 (34%)} _{-0.07835 (24%)}	13.4%
	σ_{NLO} [fb]	0.5018(3) ^{+0.0083 (1.2%)} _{-0.0337 (6.7%)}	0.4301(2) ^{+0.0035 (0.8%)} _{-0.0264 (6.1%)}	14.3%
	$\sigma_{NLO_{LOdec}}$ [fb]	—	0.4433(2) ^{+0.0323 (7.3%)} _{-0.0470 (11%)}	
	$\mathcal{K} = \sigma_{NLO}/\sigma_{LO}$	1.31	1.30 (LOdec: 1.34)	

$\alpha_{CP} = 0, \pi/4$ and $\pi/2$. We do this comparison only for a few values of α_{CP} and fixed κ_{HVV} and $\kappa_{At\bar{t}}$ since equation (4.2) does not hold at one-loop level for the full off-shell calculation, making a simple interpolation impossible at NLO. Following the argumentation of Ref. [48], we will henceforth use $\kappa_{HVV} = 1$ and $\kappa_{At\bar{t}} = 2/3$ in order to be consistent with ATLAS and CMS measurements since we focus here on a potential non-zero mixing angle α_{CP} for the SM Higgs boson.

Just like at LO, the off-shell effects at NLO increase for larger values of α_{CP} . For the SM case we find that the full off-shell results at LO and NLO in QCD are slightly smaller than those obtained using the NWA. Specifically, the full top-quark and W boson off-shell effects change the integrated LO and NLO fiducial cross-section by about 0.4%. The finding is consistent with the expected uncertainty of the NWA [99], which for sufficiently inclusive observables is of the order of $\mathcal{O}(\Gamma_t/m_t) \sim 0.8\%$. It is the other way around for \mathcal{CP} -mixed and \mathcal{CP} -odd Higgs boson production. In these two cases the NWA results are smaller than the full off-shell ones. Moreover, the full off-shell effects are of the order of 0.7%–0.9% (13%–14%) for the \mathcal{CP} -mixed (\mathcal{CP} -odd) case. Even at the level of integrated fiducial cross-sections, off-shell effects for the pure \mathcal{CP} -odd case are substantial and therefore easily distinguishable from the other two cases. A similar pattern will be visible at the differential cross-section level.

Concerning the NLO QCD corrections we find that these are positive for all three values of α_{CP} and consistent between the NWA and full off-shell results. Similarly to the off-shell effects, they increase with larger mixing angle, albeit not as drastically. For the \mathcal{CP} -even and -mixed scenarios we find corrections of 21% – 23% while they are at the level of 30% – 31% for the \mathcal{CP} -odd case. Scale uncertainties for the \mathcal{CP} -even and -mixed cases, taken as the maximum of the lower and upper bounds, amount to 31% at LO. After the inclusion of NLO QCD corrections, they are reduced substantially to 5%. For the \mathcal{CP} -odd case theoretical uncertainties arising from the scale dependence are of the order of 34% at LO and 6% – 7% at NLO. Thus, by including higher-order effects in α_s we have reduced the theoretical error by a factor of 6.

In Table 2 we additionally provide results for the $\text{NWA}_{\text{LOdec}}$, i.e. for the NWA with NLO QCD corrections to the production stage and with LO top-quark decays (denoted as $\sigma_{\text{NLO}_{\text{LOdec}}}$ in Table 2). In line with previous findings for top-quark pair associated production with γ , H , W^\pm and Z bosons [52, 60, 70, 100, 101] we observe that $\text{NWA}_{\text{LOdec}}$ predictions are higher compared to the NLO QCD results in the full NWA. Specifically, for the process at hand we have an increase of 3% – 5%. The difference is largest for the \mathcal{CP} -even and smallest for the \mathcal{CP} -odd Higgs boson. The corresponding \mathcal{K} -factors, defined as $\mathcal{K} = \sigma_{\text{NLO}_{\text{LOdec}}}/\sigma_{\text{LO}}$, are included in Table 2 in parenthesis. We observe that not only the size of higher-order corrections is amplified in this case, but also the associated scale uncertainties are larger. Due to the lack of higher-order effects in top-quark decays the latter amount to 9% – 11%.

Finally, let us also mention that, as expected from $t\bar{t}H$ production with stable top quarks, we find that the mixing term σ_3 in Eq. (4.2) between the \mathcal{CP} -even and \mathcal{CP} -odd states vanishes also for the NLO QCD predictions in the full NWA as well as for the case with LO top-quark decays. Indeed, we can write

$$\sigma(\alpha_{CP} = \pi/4) = \frac{1}{2} \{ \sigma(\alpha_{CP} = 0) + \sigma(\alpha_{CP} = \pi/2) \}, \quad (4.4)$$

which is fulfilled within statistical uncertainties for both cases (see Table 2).

5 Differential fiducial cross-sections

In this section we perform the comparison between the \mathcal{CP} -even (SM), \mathcal{CP} -mixed and \mathcal{CP} -odd Higgs boson at the differential level. In the first step, we analyse the impact of NLO QCD corrections on various differential cross-section distributions for the three \mathcal{CP} cases. Subsequently, the size of off-shell and higher-order effects in top-quark decays is discussed.

In Figures 3 and 4 we present differential distributions for dimensionful observables, specifically the transverse momentum of the Higgs boson ($p_{T,H}$), the total missing transverse momentum ($p_{T,miss}$), the transverse momentum of the hardest b -jet (p_{T,b_1}), the transverse momentum of the muon (p_{T,μ^-}), the invariant mass of the two b -jets ($M_{b_1b_2}$) and the minimum mass of the positron and a b -jet ($M_{(be^+)_{min}}$). In the upper panels of each plot the differential cross-section distributions are given for the SM, \mathcal{CP} -mixed and \mathcal{CP} -odd Higgs boson. Moreover, as reference, we display the theoretical uncertainties obtained by scale variation for the SM Higgs boson. The lower panels show the differential \mathcal{K} -factor for all three \mathcal{CP} states. For $p_{T,H}$ we observe that the relative QCD corrections are very similar for the SM, \mathcal{CP} -mixed and \mathcal{CP} -odd Higgs boson. They are about 9% – 12% at the beginning of the spectrum, whereas towards the tails they increase up to 45%. In contrast, the QCD corrections for $p_{T,miss}$ behave quite differently for the \mathcal{CP} -odd Higgs boson and increase from 28% to 45% for increasing transverse momenta. For the other two \mathcal{CP} configurations, the QCD corrections rise more drastically from 15% at the beginning up to 60% in the tail. Generally, in the case of $t\bar{t}$ production, p_T observables

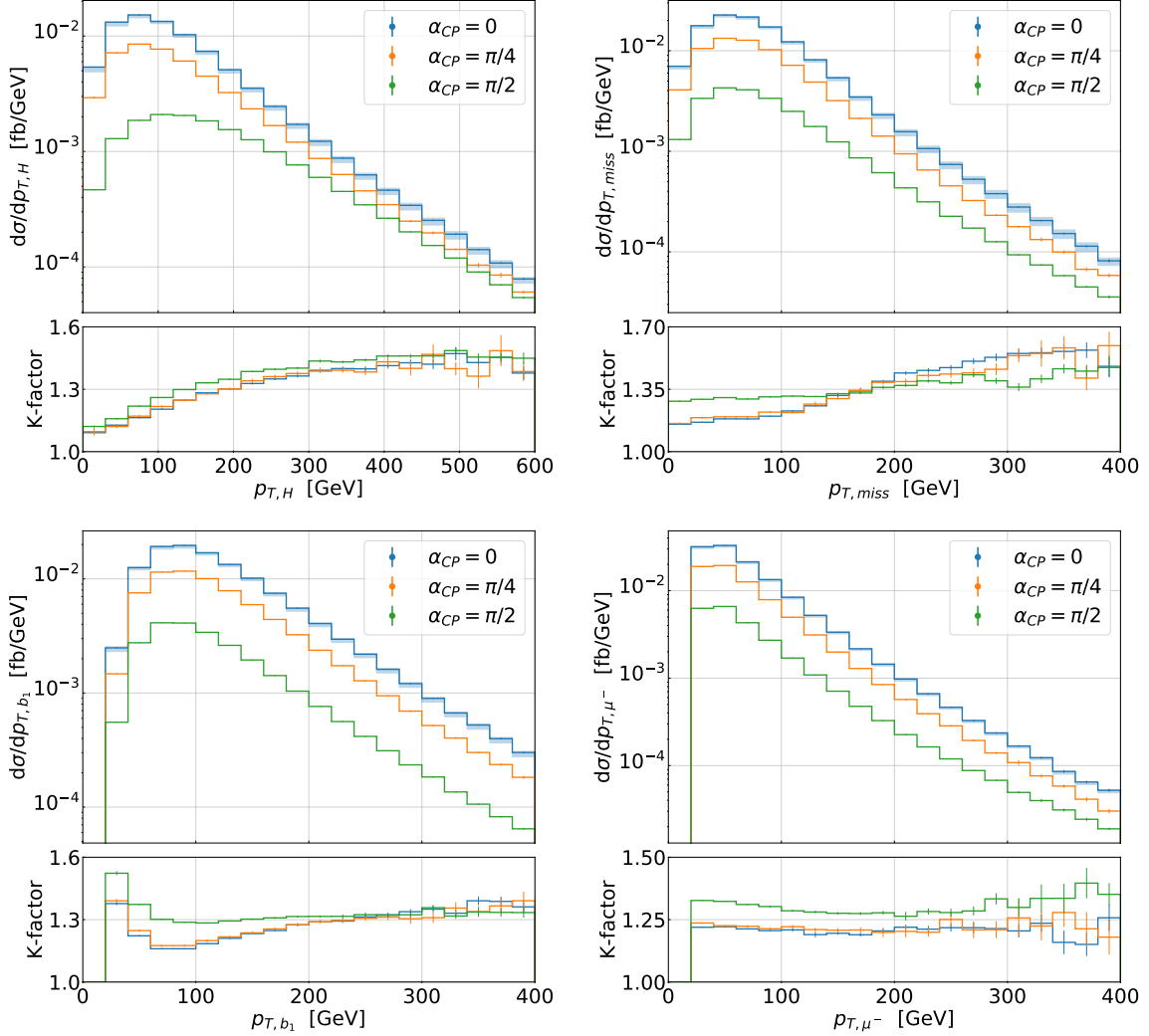


Figure 3: *Differential distributions at NLO in QCD for $\alpha_{CP} = 0, \pi/4, \pi/2$ for the observables $p_{T,H}$, $p_{T,miss}$, p_{T,b_1} and p_{T,μ^-} for the $pp \rightarrow e^+ \nu_e \mu^- \bar{\nu}_\mu b \bar{b} H$ process at the LHC with $\sqrt{s} = 13$ TeV. The lower panels show the differential \mathcal{K} -factor. Scale uncertainties are given for $\alpha_{CP} = 0$ in the upper panel while Monte Carlo integration errors are displayed in both panels.*

constructed from the decay products of both top quarks, like for example $p_{T,miss}$, $p_{T,b_1 b_2}$ and $p_{T,e^+ \mu^-}$, are known to have huge \mathcal{K} -factors in the tails, see e.g. [58, 102]. At LO these observables exhibit a strong suppression of the $t\bar{t}$ cross-section above 150 GeV. In the case of the dominant double-resonant top-quark contributions, top-quark decay products are boosted via their parents, which have opposite momenta. Even though the transverse momentum of the particular decay products can be substantial, the p_T of the $b\bar{b}$, $e^+ \mu^-$ and $\nu_e \bar{\nu}_\mu$ systems can only acquire rather small values. At NLO the $t\bar{t}$ system can attain large transverse momentum by recoiling against extra jet radiation. Thus, the kinematical constraint is partially lifted resulting in an enhancement of the NLO cross-section and a huge \mathcal{K} -factor of 2 – 4. For the $t\bar{t}H$ production, where radiation of the Higgs boson off top quarks is already taking place at LO, smaller NLO corrections are foreseen. Indeed, the latter generate \mathcal{K} -factors in the range of 1.6 – 1.8 [51, 52]. Additionally, the harder Higgs boson spectrum in the \mathcal{CP} -odd case leads to a relaxation of the kinematical suppression already at LO for $p_{T,miss}$. Similar higher-order

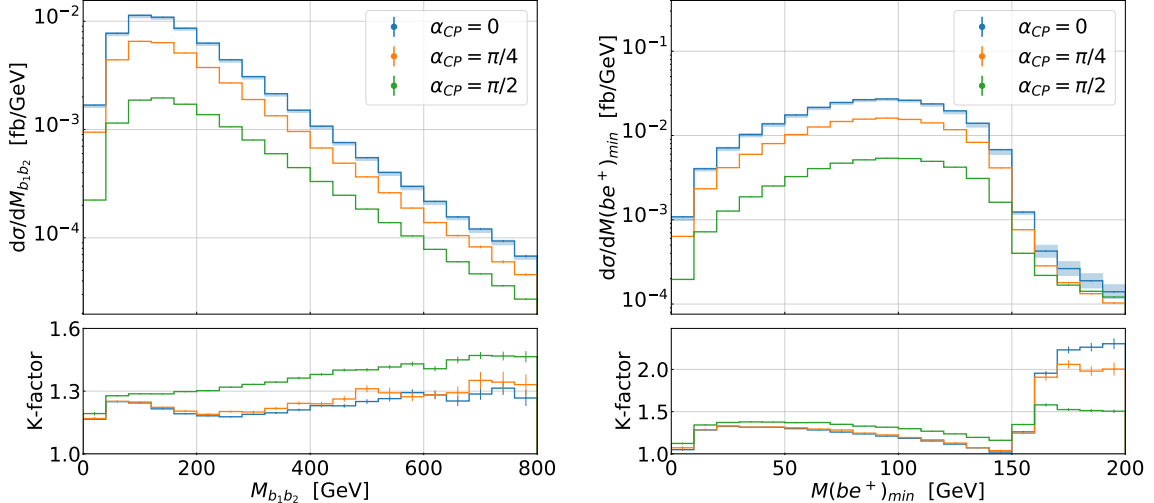


Figure 4: Differential distributions at NLO in QCD for $\alpha_{CP} = 0, \pi/4, \pi/2$ for the observables $M_{b_1 b_2}$ and $M(be^+)_{min}$ for the $pp \rightarrow e^+ \nu_e \mu^- \bar{\nu}_\mu b \bar{b} H$ process at the LHC with $\sqrt{s} = 13$ TeV. The lower panels show the differential \mathcal{K} -factor. Scale uncertainties are given for $\alpha_{CP} = 0$ in the upper panel while Monte Carlo integration errors are displayed in both panels.

effects are observed for $p_{T, b_1 b_2}$ and $p_{T, e^+ \mu^-}$. For p_{T, b_1} we again find an enhancement of the NLO QCD corrections at the beginning of the spectrum for the \mathcal{CP} -odd Higgs boson leading to effects up to 52% compared to 40% for the other \mathcal{CP} configurations. These differences decrease towards the high p_T -region and we observe $\mathcal{O}(\alpha_s)$ corrections up to 40% for all three cases. For p_{T, μ^-} we find NLO QCD corrections of about 20% – 25% for the SM and \mathcal{CP} -mixed Higgs boson while they increase up to 25% – 35% for the \mathcal{CP} -odd one. For all three \mathcal{CP} configurations, the higher-order effects mainly impact the normalisation and we do not observe significant shape distortions. The QCD corrections for the differential distribution $M_{b_1 b_2}$ are very similar for all three \mathcal{CP} configurations at the beginning of the spectrum and amount to 25% – 28%. Towards the tail they increase up to 45% for the \mathcal{CP} -odd Higgs boson and up to 30% – 35% for the other two \mathcal{CP} configurations.

In the case of on-shell top quarks and W gauge bosons, the observable $M(be^+)_{min}$ is characterised by a sharp upper bound, $\sqrt{m_t^2 - m_W^2} \approx 153$ GeV, which renders it very sensitive to the top-quark mass. Due to additional radiation, this kinematical edge is smeared at NLO in QCD for the NWA. For the off-shell prediction, small but non-negligible single- and non-resonant contributions that elude the kinematical bound around 153 GeV are already present at LO. Thus, this observable is particularly interesting for investigating the top-quark modeling. At NLO this feature becomes more pronounced because of QCD radiation that enters the b -jet without being emitted from its parent b quark. As a result, we find very significant higher-order effects both below and above this kinematical bound. Additionally, we observe that the QCD corrections are very similar for small invariant masses while towards the kinematical edge around 153 GeV the \mathcal{CP} -odd Higgs boson leads to 12% – 15% larger QCD corrections. The QCD corrections increase significantly for all three \mathcal{CP} configurations for invariant masses above this edge but their size differs substantially. We find the smallest QCD corrections in this region for the \mathcal{CP} -odd Higgs boson at about 50% while they increase even further to 100% for the \mathcal{CP} -mixed case and to 130% for the SM Higgs boson which means that the enhancement due to real radiation above this kinematical edge is significantly reduced in the \mathcal{CP} -odd case. As we have already

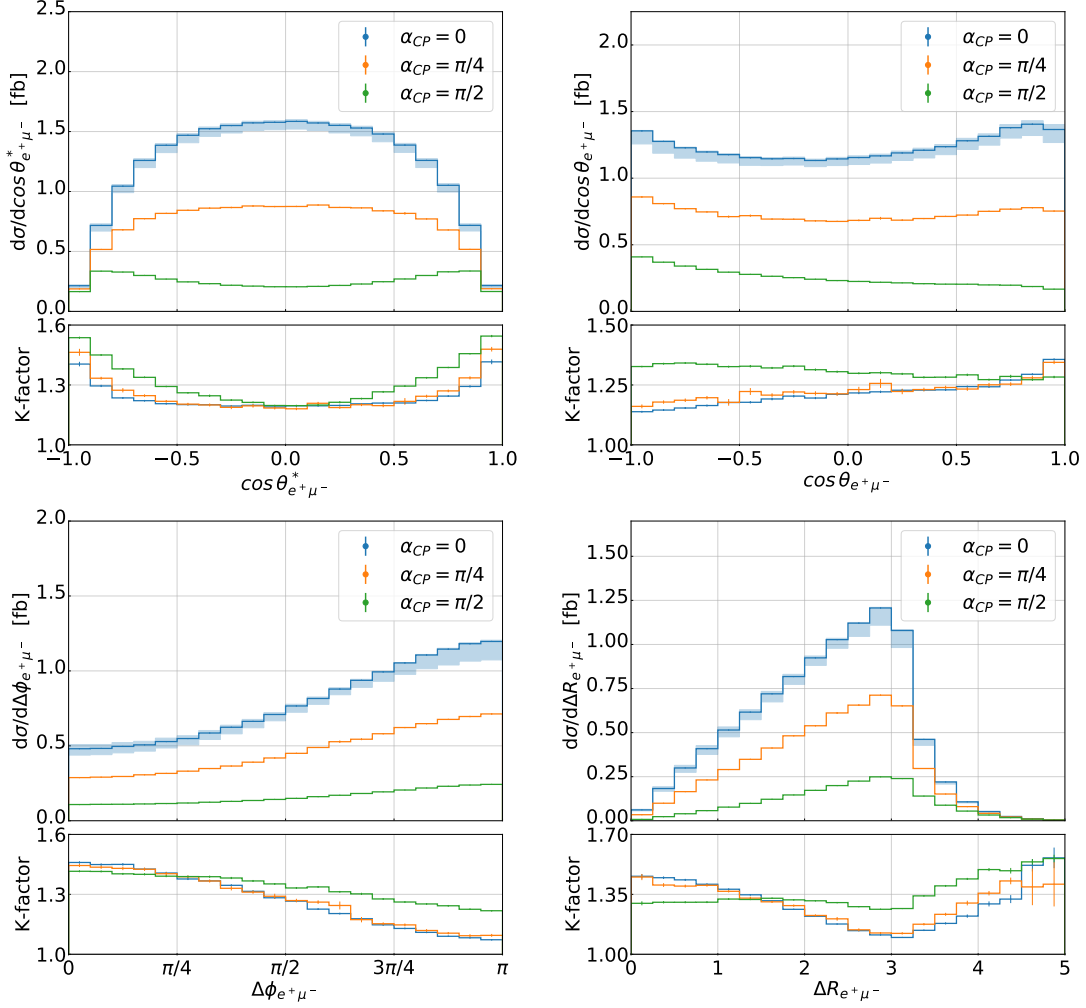


Figure 5: *Differential distributions at NLO in QCD for $\alpha_{CP} = 0, \pi/4, \pi/2$ for the observables $\cos \theta_{e^+\mu^-}^*$, $\cos \theta_{e^+\mu^-}$, $\Delta \phi_{e^+\mu^-}$ and $\Delta R_{e^+\mu^-}$ for the $pp \rightarrow e^+ \nu_e \mu^- \bar{\nu}_\mu b \bar{b} H$ process at the LHC with $\sqrt{s} = 13$ TeV. The lower panels show the differential \mathcal{K} -factor. Scale uncertainties are given for $\alpha_{CP} = 0$ in the upper panel while Monte Carlo integration errors are displayed in both panels.*

seen at the level of integrated cross-sections (Table 2), the relative size of full off-shell effects and, in turn, the contribution from HVV couplings, are significantly larger than for the other two \mathcal{CP} states. Also here the single- and non-resonant contributions play a crucial role since they are less affected by this kinematical edge and thus typically receive smaller QCD corrections than the double-resonant part in this phase-space region.

In Figures 5 and 6 we show the differential distributions and differential \mathcal{K} -factors for the dimensionless observables $\cos \theta_{e^+\mu^-}^*$, the cosine of the opening angle between the two charged leptons ($\cos \theta_{e^+\mu^-}$), the azimuthal angle between the two charged leptons ($\Delta \phi_{e^+\mu^-}$), the distance in the azimuthal angle rapidity plane between two charged leptons ($\Delta R_{e^+\mu^-}$), the rapidity of the muon (y_{μ^-}) and the rapidity of the Higgs boson (y_H). The observable $\cos \theta_{e^+\mu^-}^*$ has been introduced in Ref. [103] and is defined as

$$\cos \theta_{e^+\mu^-}^* = \tanh \left(\frac{y_{e^+} - y_{\mu^-}}{2} \right). \quad (5.1)$$

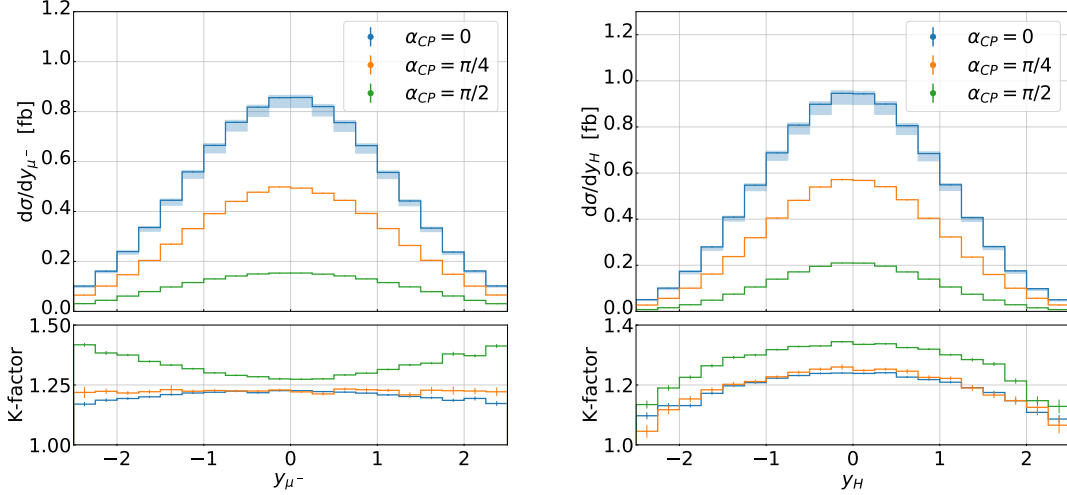


Figure 6: *Differential distributions at NLO in QCD for $\alpha_{CP} = 0, \pi/4, \pi/2$ for the observables y_{μ^-} and y_H for the $pp \rightarrow e^+ \nu_e \mu^- \bar{\nu}_\mu b \bar{b} H$ process at the LHC with $\sqrt{s} = 13$ TeV. The lower panels show the differential K -factor. Scale uncertainties are given for $\alpha_{CP} = 0$ in the upper panel while Monte Carlo integration errors are displayed in both panels.*

It should be distinguished from $\cos \theta_{e+\mu^-} = \hat{p}_{e^+} \cdot \hat{p}_{\mu^-}$ which we also use in the following. We note that $\cos \theta_{e+\mu^-}^*$ can be used to determine the \mathcal{CP} nature of spin-0 mediators in associated production of dark matter and $t\bar{t}$ pairs, see e.g. [96, 100]. For this observable we find that the NLO QCD corrections for the SM and \mathcal{CP} -mixed Higgs boson again behave rather similarly. They amount to about 20% for $\cos \theta_{e+\mu^-}^* \approx 0$ and increase towards $\cos \theta_{e+\mu^-}^* \approx \pm 1$ up to 40% for the SM and 45% for the \mathcal{CP} -mixed case. We find the same general behaviour for the \mathcal{CP} -odd Higgs boson. However, in this case the higher-order corrections can even reach 55%. The differences between LO and NLO distributions for $\cos \theta_{e+\mu^-}$ are very similar for all three \mathcal{CP} configurations for small opening angles between the two charged leptons and amount to 30% – 35% for these configurations. In the case of the SM and \mathcal{CP} -mixed Higgs boson they decrease for increasing opening angle down to 15% while they remain almost constant for the \mathcal{CP} -odd case. The rather similar behaviour of the NLO QCD corrections in the \mathcal{CP} -even and \mathcal{CP} -mixed Higgs boson cases is also present in the $\Delta \phi_{e+\mu^-}$ distributions. Here, the corrections decrease with rising opening angle from about 40% – 45% around $\Delta \phi_{e+\mu^-} \approx 0$ to 10% for $\Delta \phi_{e+\mu^-} \approx \pi$. For the \mathcal{CP} -odd Higgs boson, higher-order corrections lead to similar differences between the LO and NLO distributions for small angles, but these effects decrease less substantially and only down to 20% for larger angles. Thus, shape distortions are less pronounced for the pure pseudo-scalar Higgs boson case. For $\Delta R_{e+\mu^-}$, the $\mathcal{O}(\alpha_s)$ corrections for the \mathcal{CP} -odd Higgs boson are rather flat up to about $\Delta R_{e+\mu^-} \approx 3$, whereas for $\Delta R_{e+\mu^-} > 3$ they increase from 30% to 55%. On the other hand, we observe significant shape distortions over the whole range for the SM and \mathcal{CP} -mixed Higgs boson where the NLO QCD corrections vary between 10% and 45% – 55%. Finally, for both rapidity distributions y_{μ^-} and y_H , the higher-order QCD effects for the \mathcal{CP} -odd case exceed the ones for the SM and \mathcal{CP} -mixed Higgs boson over the entire range by up to 20% for y_{μ^-} and 10% for y_H . The SM and \mathcal{CP} -mixed cases obtain higher-order corrections of about 20% – 25% for y_{μ^-} while they vary between 10% and 25% for y_H .

Concluding, the NLO QCD corrections for the SM (\mathcal{CP} -even) and \mathcal{CP} -mixed case are comparable for most of the observables we have examined. A similar behaviour has already been found at the

integrated fiducial level for these two cases. Just like at the integrated level, the $\mathcal{O}(\alpha_s)$ corrections for the \mathcal{CP} -odd Higgs are larger than for the other two cases. Indeed, the harder Higgs-boson radiation for the pure pseudo-scalar case as compared to the SM Higgs boson has an important impact on the size and shape of the higher-order QCD corrections for dimensionful and dimensionless observables. This is especially visible for observables which obtain large NLO QCD corrections due to additional radiation.

In the next step we discuss the shape distortions due to the different Higgs boson \mathcal{CP} configurations and the size of full off-shell effects. The latter analysis is performed by comparing the full off-shell calculation to the NWA predictions. In this way we can estimate the impact of off-shell effects on dimensionful and dimensionless observables for the three different \mathcal{CP} states. We start this discussion with the four dimensionful observables H_T , $p_{T,H}$, $M(be^+)_{min}$ and $M_{T2,t}$ shown in Figure 7. In the upper panels we give the differential distributions for the SM (\mathcal{CP} -even), \mathcal{CP} -mixed and \mathcal{CP} -odd Higgs boson in the full off-shell calculation (solid lines) and in the NWA (dashed lines). The middle panels provide the ratio to the $\alpha_{CP} = 0$ case for the normalised differential distributions in the full off-shell approach. The ratio NWA/off-shell for each α_{CP} value is displayed in the lower panels. The scale uncertainties are provided as reference for the SM case in the two upper panels while Monte Carlo errors are reported in all three panels. For H_T , as defined in Eq. (3.6), we find that compared to the SM Higgs boson, the spectra for the \mathcal{CP} -mixed and \mathcal{CP} -odd case are harder towards the tails. Specifically, we find an increase of only about 10% for the \mathcal{CP} -mixed case while for the \mathcal{CP} -odd case the increase is very significant with more than 100%. In both cases these effects are larger than the corresponding scale uncertainties for the \mathcal{CP} -even case which only amount to up to 6%. The full off-shell effects for the SM and \mathcal{CP} -mixed Higgs boson cases are very similar to each other and amount to about 5% in the tails which is comparable to the size to the scale uncertainties. On the other hand, we obtain large off-shell effects of about 45% for the \mathcal{CP} -odd Higgs boson. The latter exceed the full off-shell effects at the integrated level by more than a factor of three. Since these off-shell effects rise towards the tails, they also have a significant impact on the normalised ratios shown in the middle panels. Had we taken the NWA predictions instead of the full off-shell ones, the differences between the \mathcal{CP} states would only be up to 60% in the tails instead of about 120%. The shape differences in the tails of $p_{T,H}$ are even larger than for H_T . In particular, we observe differences with respect to the SM case at the level of 30% for the \mathcal{CP} -mixed and effects larger than 200% for the \mathcal{CP} -odd Higgs boson. Thus, these differences are significant when compared to the scale uncertainties of about 10% for the SM Higgs boson case. Consequently, the $p_{T,H}$ observable is an excellent example of a dimensionful differential cross-section distribution that might be employed to decipher the \mathcal{CP} quantum numbers of the Higgs boson and look for any hints of new physics in the Higgs-top sector. In addition, the off-shell effects are of the order of 5% for the SM and \mathcal{CP} -mixed case and thus would not have an impact on this comparison. For the \mathcal{CP} -odd case, on the other hand, the full off-shell effects increase up to 35% in the tails of the $p_{T,H}$ distribution rendering them indispensable in studies of the \mathcal{CP} state of the Higgs boson. If we had set $\kappa_{H\bar{t}t} = \kappa_{A\bar{t}t} = 1$ instead, then the absolute differential distributions for $p_{T,H}$ would coincide in the tails for all three \mathcal{CP} cases in the NWA, see e.g. Refs. [41, 45]. Taking into account the fragmentation functions in Eq. (4.3), this behaviour becomes clear since the soft enhancement for the scalar Higgs boson is absent in the tails of this distribution. On the other hand, in the full off-shell calculation we would not obtain such a behaviour due to the large effects coming from single- and non-resonant top-quark contributions as well as their interference effects with double-resonant ones. For $M(be^+)_{min}$ the SM and \mathcal{CP} -mixed Higgs boson cases lead to the exact same normalised distributions below the kinematical edge around $M(be^+)_{min} \approx 153$ GeV. Above this edge the difference between the

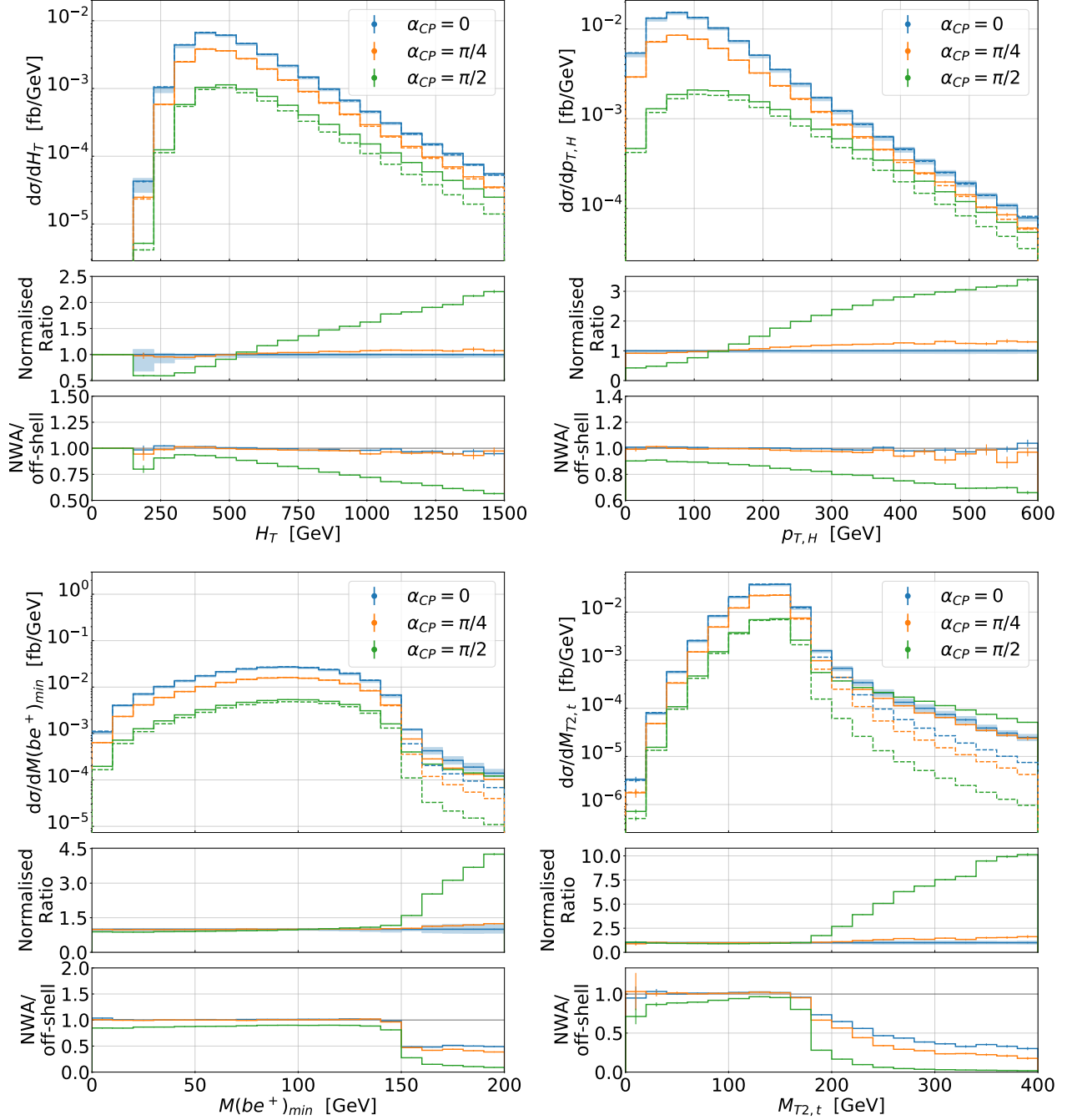


Figure 7: Differential distributions at NLO in QCD for $\alpha_{CP} = 0, \pi/4, \pi/2$ for the observables H_T , $p_{T,H}$, $M(\text{be}^+)_{\min}$ and $M_{T2,t}$ for the $pp \rightarrow e^+ \nu_e \mu^- \bar{\nu}_\mu b \bar{b} H$ process at the LHC with $\sqrt{s} = 13$ TeV. The upper panels show full off-shell and NWA (dashed lines) results. The middle panels provide the ratio to $\alpha_{CP} = 0$ of the normalised differential distributions for the full off-shell case. The ratio NWA/off-shell is given in the lower panels. Scale uncertainties are shown for $\alpha_{CP} = 0$ in the upper and middle panels while Monte Carlo integration errors are displayed in all panels.

two scenarios is in the 20% – 25% range. Nevertheless, it is still comparable to the scale uncertainties of the \mathcal{CP} -even case, which are of the order of 20% in this phase-space region. In the \mathcal{CP} -odd case

the ratio of the normalised differential distribution to the SM distribution is larger than four. Even the absolute differential cross-section distribution for the \mathcal{CP} -odd case is larger than the \mathcal{CP} -mixed one in this phase-space region, even though the overall normalisation is almost three times smaller. This behaviour is closely related to the size of the full off-shell effects, which reach up to 90% for the \mathcal{CP} -odd Higgs boson but only 50% for the SM and 60% for the \mathcal{CP} -mixed Higgs boson. This is a result of a larger relative contribution from single- and non-resonant diagrams for the \mathcal{CP} -odd Higgs boson which is partially caused by the non-vanishing HVV coupling. A similar phenomenon can be observed in the transverse mass $M_{T2,t}$ [104–106] which is a generalisation of the transverse mass in case of pairs of unstable particles and is defined as

$$M_{T2,t}^2 = \min_{\mathbf{p}_T^{\nu_1} + \mathbf{p}_T^{\nu_2} = \mathbf{p}_{T,miss}} \left[\max \left\{ M_T^2 \left(\mathbf{p}_T^{(lb)1}, \mathbf{p}_T^{\nu_1} \right), M_T^2 \left(\mathbf{p}_T^{(lb)2}, \mathbf{p}_T^{\nu_2} \right) \right\} \right], \quad (5.2)$$

where the transverse mass of the lepton+ b -jet system in presence of a missing transverse momentum $\mathbf{p}_T^{\nu_i}$ is given by

$$M_T^2 \left(\mathbf{p}_T^{(lb)_i}, \mathbf{p}_T^{\nu_i} \right) = M_{(lb)_i}^2 + 2 \left(E_T^{(lb)_i} E_T^{\nu_i} - \mathbf{p}_T^{(lb)_i} \cdot \mathbf{p}_T^{\nu_i} \right). \quad (5.3)$$

We choose the lepton+ b -jet pairs by minimising the value $Q = M_{e+b_i} + M_{\mu-b_j}$ so that we do not take into account the charge of the b -jets. Similarly to $M(be^+)_{min}$, the transverse mass has a kinematical edge around the top-quark mass ($m_t = 172.5$ GeV). For $M_{T2,t} > m_t$, large suppression of double-resonant top-quark contributions occurs. Thus, the absolute value of the cross-section is significantly reduced above this edge and the full off-shell effects, which are driven by the single-resonant top-quark contributions, increase. Following the same reasoning as before, this reduction is suppressed for the \mathcal{CP} -odd case. When examining the absolute differential cross-section distributions we can observe that the \mathcal{CP} -odd case exceeds even the SM results in these phase-space regions. The difference between the normalised $M_{T2,t}$ distributions can reach a factor of 10. A less significant enhancement occurs for the \mathcal{CP} -mixed Higgs boson so that the SM and \mathcal{CP} -mixed cases are very similar towards the end of the absolute $M_{T2,t}$ spectrum. This is due to the large shape differences of about 50% – 60% which are substantial compared to the scale uncertainties. The latter are in the 15% – 18% range for the \mathcal{CP} -even case. Compared to the $M(be^+)_{min}$ differential cross-section distribution the full off-shell effects are even larger here. Indeed, they are of the order of 70%, 80% and 98% for the \mathcal{CP} -even, \mathcal{CP} -mixed and \mathcal{CP} -odd case, respectively. Both $M(be^+)_{min}$ and $M_{T2,t}$ are very sensitive to the various Higgs boson \mathcal{CP} numbers. However, they are also subject to large off-shell effects. Not only the finite top-quark width effects should be properly taken into account for these observables but also single-resonant top-quark contributions and interference effects must be incorporated to adequately describe the phase-space regions above these kinematical edges.

In the next step we discuss the shape differences between the \mathcal{CP} -even, \mathcal{CP} -mixed and \mathcal{CP} -odd Higgs boson as well as the respective size of off-shell effects in several angular observables. In Figure 8 we present the differential cross-section distributions for $\cos \theta_{e^+\mu^-}^*$, $\cos \theta_{e^+\mu^-}$, $\cos \theta_{b_1 b_2}^*$ and $\cos \theta_{b_1 b_2}$. In the case of $\cos \theta_{e^+\mu^-}^*$ we find that the prediction for the central value of the scale is smaller by about 7% for the \mathcal{CP} -mixed and 35% for \mathcal{CP} -odd Higgs boson compared to the SM case. These differences increase significantly towards $\cos \theta_{e^+\mu^-}^* \approx \pm 1$ to about 50% for the \mathcal{CP} -mixed and more than 200% for the \mathcal{CP} -odd case. Thus, the two leptons tend to be more separated in the rapidity plane in the case of the \mathcal{CP} -mixed and \mathcal{CP} -odd Higgs boson. Furthermore, the theoretical uncertainties due to the scale dependence are not only very small but also very similar for all the four observables. More specifically, we have theoretical uncertainties at the level of 5% in the central regions for the SM Higgs boson case, whereas towards $\cos \theta_{e^+\mu^-}^* \approx \pm 1$ they increase only slightly up to 7% – 9%. This means that the shape differences outlined above are much larger than the scale uncertainties. As a result, we can conclude

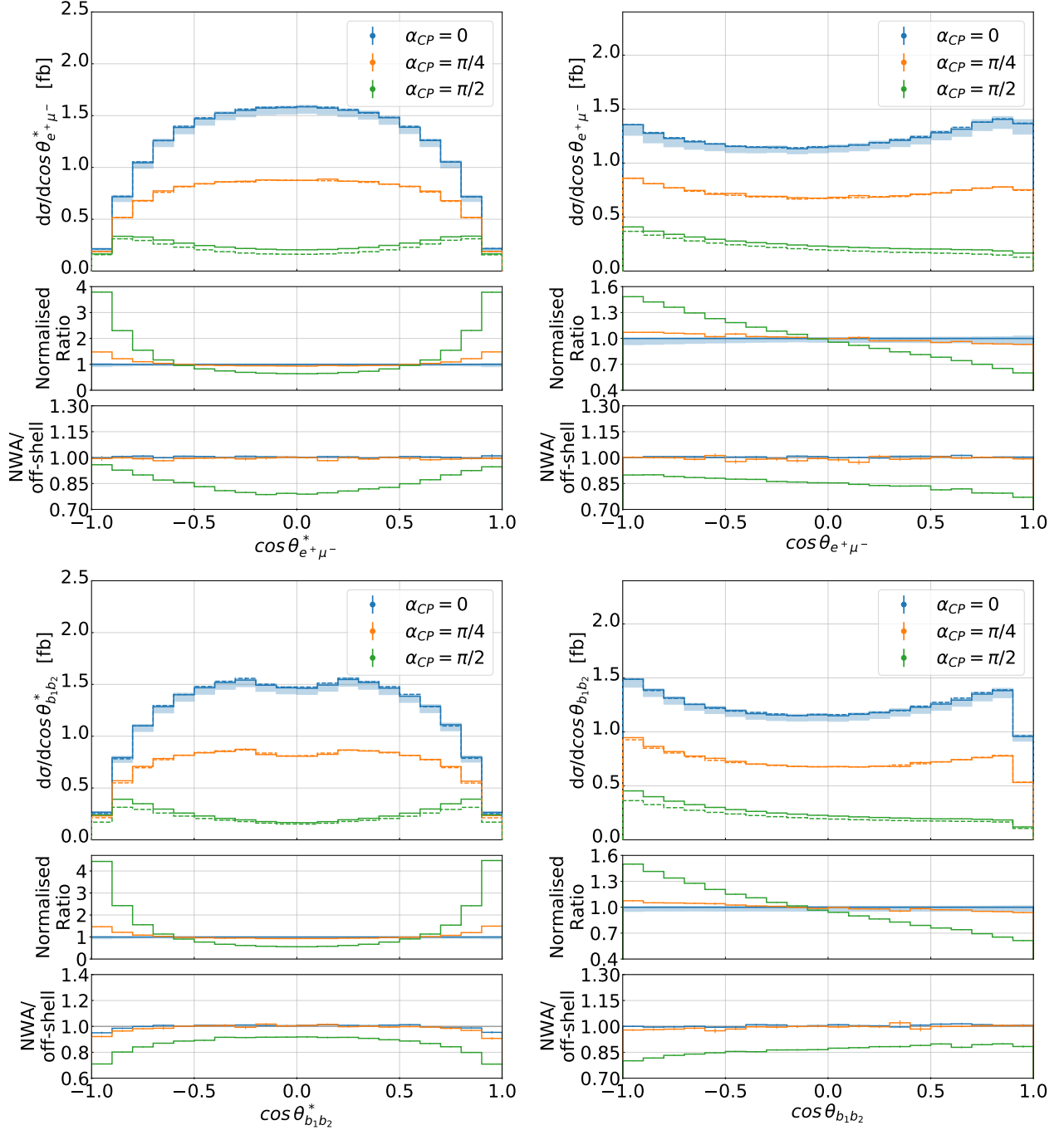


Figure 8: Differential distributions at NLO in QCD for $\alpha_{CP} = 0, \pi/4, \pi/2$ for the observables $\cos\theta_{e^+\mu^-}^*$, $\cos\theta_{e^+\mu^-}$, $\cos\theta_{b_1b_2}^*$ and $\cos\theta_{b_1b_2}$ for the $pp \rightarrow e^+\nu_e\mu^-\bar{\nu}_\mu b\bar{b}H$ process at the LHC with $\sqrt{s} = 13$ TeV. The upper panels show full off-shell and NWA (dashed lines) results. The middle panels provide the ratio to $\alpha_{CP} = 0$ of the normalised differential distributions for the full off-shell case. The ratio NWA/off-shell is given in the lower panels. Scale uncertainties are shown for $\alpha_{CP} = 0$ in the upper and middle panels while Monte Carlo integration errors are displayed in all panels.

that the $\cos\theta_{e^+\mu^-}^*$ angular differential cross-section distribution is a promising \mathcal{CP} -sensitive observable to be measured at the LHC. This is further underlined when examining the full off-shell effects for

the SM and \mathcal{CP} -mixed Higgs boson. We can observe that these effects are less than 2% in both cases. Thus, they are even comparable in size to the full off-shell top-quark effects at the integrated fiducial cross-section level. However, the situation is rather different for the \mathcal{CP} -odd Higgs boson for which the off-shell effects lead to a wrong normalisation as well as additional shape distortions and we find that the off-shell effects are reduced from the centre of the plot towards the edges from 20% to 5%. Thus, even for angular distributions, single- and non-resonant contributions can significantly affect the shape, especially in the $\cos\theta_{e^+\mu^-}^* \approx 0$ phase-space region where theoretical uncertainties are four times smaller than the size of the full off-shell effects. Consequently, the latter should be included in theoretical predictions when comparing to experimental LHC data. For $\cos\theta_{e^+\mu^-}$ we can see the largest differences between the SM and the \mathcal{CP} -mixed Higgs boson around $\cos\theta_{e^+\mu^-} \approx \pm 1$. At about 7%, they are comparable in size to the scale uncertainties in those phase-space regions. The situation is again quite different for the \mathcal{CP} -odd Higgs boson. In this case, differences of up to 40% – 50% are obtained for $\cos\theta_{e^+\mu^-} \approx \pm 1$. The off-shell effects for the SM and \mathcal{CP} -mixed Higgs boson cases are again quite small and rather similar in size while for the \mathcal{CP} -odd one they significantly affect the normalisation and shape of the distribution. In particular, the off-shell effects reduce towards large opening angles from 20% to 10%.

The observables $\cos\theta_{b_1b_2}^*$ and $\cos\theta_{b_1b_2}$, which are the hadronic counterparts of the two previously discussed observables, are important for leptonic Higgs boson decays since in those cases we have a larger lepton multiplicity which makes a precise measurement of leptonic observables more challenging. All in all, the shape differences between the three \mathcal{CP} states are similar to those of the leptonic observables. This is especially true for $\cos\theta_{b_1b_2}$ for which the normalised ratios are essentially the same as for $\cos\theta_{e^+\mu^-}$. For the \mathcal{CP} -odd Higgs boson, on the other hand, both the $\cos\theta_{b_1b_2}^* \approx 0$ and $\cos\theta_{b_1b_2}^* \approx \pm 1$ phase-space regions receive additional enhancements. Compared to the corresponding scale uncertainties the off-shell effects of the \mathcal{CP} -even and \mathcal{CP} -mixed Higgs boson are again negligible for both observables but sizable for the \mathcal{CP} -odd case. In the latter case, they amount to 10% – 30% for $\cos\theta_{b_1b_2}^*$ and 10% – 20% for $\cos\theta_{b_1b_2}$ which substantially exceed the corresponding theoretical uncertainties and lead to significant shape distortions.

In the following, we investigate the contribution of double-, single- and non-resonant fiducial phase-space regions to the integrated and differential cross-sections for the full off-shell case. This should give us a qualitative picture of the importance of the individual contributions, as well as their general distribution for a given value of the \mathcal{CP} -mixing angle of the Higgs boson. To identify these contributions, we use the method introduced in Ref. [107]. This approach was further modified and employed in various studies, see e.g. [60, 108–110]. Specifically, at NLO in QCD we have the following three resonance histories

$$\begin{aligned}
\text{(i)} \quad & t = W^+(\rightarrow e^+\nu_e)b & \text{and} & \quad \bar{t} = W^-(\rightarrow \mu^-\bar{\nu}_\mu)\bar{b}, \\
\text{(ii)} \quad & t = W^+(\rightarrow e^+\nu_e)bj & \text{and} & \quad \bar{t} = W^-(\rightarrow \mu^-\bar{\nu}_\mu)\bar{b}, \\
\text{(iii)} \quad & t = W^+(\rightarrow e^+\nu_e)b & \text{and} & \quad \bar{t} = W^-(\rightarrow \mu^-\bar{\nu}_\mu)\bar{b}j,
\end{aligned} \tag{5.4}$$

where the light jet (if resolved by the *anti- k_T* jet algorithm with $R = 0.4$) is added to the list only if it passes the following cuts: $|y_j| < 2.5$ and $p_{T,j} > 15$ GeV. In this way, we closely mimic what is done on the experimental side for the light jet to be observed in the ATLAS or CMS detector. For each history we compute the following quantity

$$\mathcal{Q} = |M_t - m_t| + |M_{\bar{t}} - m_t|, \tag{5.5}$$

where $m_t = 172.5$ GeV and M_t ($M_{\bar{t}}$) is the invariant mass of the reconstructed top quark (anti-top quark). For each phase-space point, one history is selected by minimising the value of \mathcal{Q} . The

Table 3: *NLO QCD integrated fiducial cross-sections as calculated in the full off-shell approach together with predictions for DR, SR and NR fiducial phase-space regions for $\alpha_{CP} = 0, \pi/4$ and $\pi/2$. Also shown are their respective Monte Carlo integration errors. All values are given for the $pp \rightarrow e^+ \nu_e \mu^- \bar{\nu}_\mu b \bar{b} H$ process at the LHC with $\sqrt{s} = 13$ TeV.*

α_{CP}	Off-shell [fb]	Double-resonant [fb]	Single-resonant [fb]	Non-resonant [fb]
0 (SM)	2.466(2)	2.246(2)	0.2138(5)	0.00594(7)
$\pi/4$	1.465(2)	1.325(2)	0.136(1)	0.0039(1)
$\pi/2$	0.5018(3)	0.4037(9)	0.0948(4)	0.00346(5)

boundaries of the fiducial double-resonant (DR), single-resonant (SR) and non-resonant (NR) regions are expressed in terms of Γ_t^{NLO} and the parameter $n = 15$. The value of the latter is rather arbitrary. The DR phase-space region is defined according to

$$|M_t - m_t| < n \Gamma_t^{\text{NLO}}, \quad \text{and} \quad |M_{\bar{t}} - m_t| < n \Gamma_{\bar{t}}^{\text{NLO}}. \quad (5.6)$$

There are two SR regions given by

$$|M_t - m_t| < n \Gamma_t^{\text{NLO}}, \quad \text{and} \quad |M_{\bar{t}} - m_t| > n \Gamma_{\bar{t}}^{\text{NLO}}, \quad (5.7)$$

or

$$|M_t - m_t| > n \Gamma_t^{\text{NLO}}, \quad \text{and} \quad |M_{\bar{t}} - m_t| < n \Gamma_{\bar{t}}^{\text{NLO}}. \quad (5.8)$$

The NR region is determined via

$$|M_t - m_t| > n \Gamma_t^{\text{NLO}}, \quad \text{and} \quad |M_{\bar{t}} - m_t| > n \Gamma_{\bar{t}}^{\text{NLO}}. \quad (5.9)$$

For the above outlined procedure, the contributions at the integrated fiducial cross-section level for these three regions for the \mathcal{CP} -even ($\alpha_{CP} = 0$), \mathcal{CP} -mixed ($\alpha_{CP} = \pi/4$) and \mathcal{CP} -odd ($\alpha_{CP} = \pi/2$) case are given in Table 3. The integrated fiducial cross-sections for all three cases are dominated by the DR contributions. For the SM and \mathcal{CP} -mixed Higgs boson, more than 90% of $\sigma_{\text{Off-shell}}^{\text{NLO}}$ comes from the DR contribution. For the \mathcal{CP} -odd Higgs boson, however, the DR contribution is reduced to 80%. A similar behaviour can be observed for the remaining fiducial phase-space regions. For both $\alpha_{CP} = 0$ and $\alpha_{CP} = \pi/4$, the SR region is of the order of 9%, while the NR regions of the phase space are completely negligible. Again, for $\alpha_{CP} = \pi/2$, the SR and NR contributions are larger at the level of 19% and 1%, respectively. Hence, in the case of the \mathcal{CP} -odd Higgs boson, the SR regions of the phase space are more substantial, which is reflected in the larger size of the full off-shell effects as we have already seen in Table 2.

We have confirmed these findings also at the differential level. In Figure 9 we display the differential cross-section distribution as a function of $M(be^+)_{\min}$ and $p_{T,H}$ for $\alpha_{CP} = 0$ and $\pi/2$. The \mathcal{CP} -mixed case is omitted as it follows the SM Higgs boson very closely. For each plot, we show the full off-shell and NWA predictions as well as the results for the DR, SR and NR fiducial phase-space regions. The lower panels display the ratio of all contributions to the full off-shell result. For the $M(be^+)_{\min}$

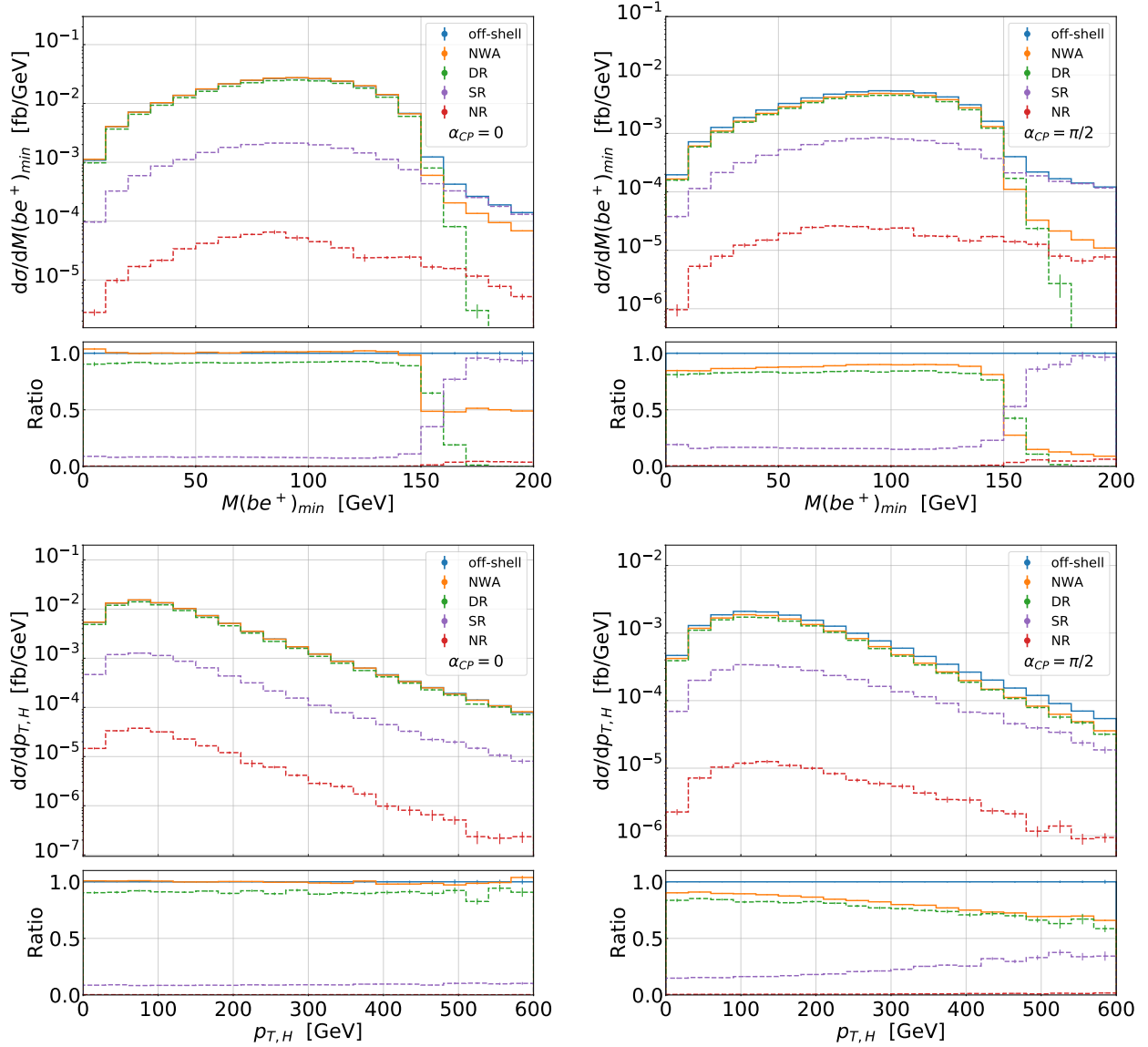


Figure 9: Differential distributions at NLO in QCD for $\alpha_{CP} = 0$ and $\pi/2$ for the observables $M(be^+)_{min}$ and $p_{T,H}$ for the $pp \rightarrow e^+\nu_e\mu^-\bar{\nu}_\mu b\bar{b}H$ process at the LHC with $\sqrt{s} = 13$ TeV. The upper panels show full off-shell and NWA results as well as predictions for DR, SR and NR fiducial phase-space regions. The ratios of all contributions to the full off-shell result are shown in the lower panels. Monte Carlo integration errors are displayed in both panels.

distribution, we observe that in the case of the \mathcal{CP} -even Higgs boson, the SR part rapidly increases in the region that starts to be sensitive to off-shell effects, i.e. for $M(be^+)_{min} \approx 153$ GeV, and even starts to dominate the full off-shell result towards the end of the spectrum. This effect is enhanced for the \mathcal{CP} -odd Higgs boson. As a matter of fact, we have the following distribution of DR, SR and NR phase-space regions for $M(be^+)_{min}$ around 153 GeV; DR 65% (42%), SR 35% (53%) and NR 1% (4%) for $\alpha_{CP} = 0$ ($\alpha_{CP} = \pi/2$). Even for $M(be^+)_{min} \leq 153$ GeV, the SR contribution for $\alpha_{CP} = \pi/2$ is twice as large as for the $\alpha_{CP} = 0$ case. A similar effect can be observed for $p_{T,H}$. Even though in the high p_T tail of the differential cross-section distribution the SR part does not dominate the full

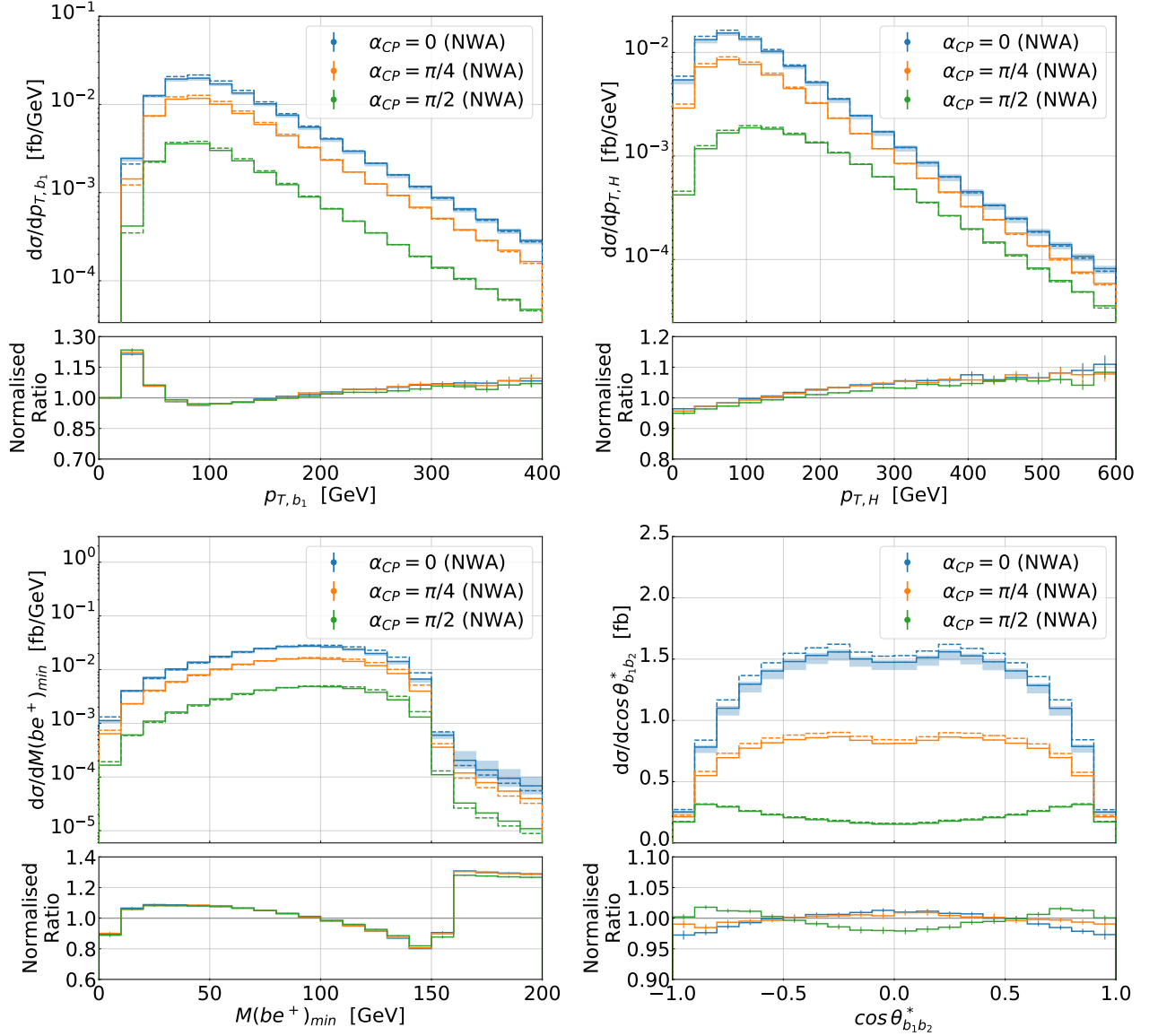


Figure 10: *Differential distributions at NLO in QCD for $\alpha_{CP} = 0, \pi/4, \pi/2$ for the observables p_{T,b_1} , $p_{T,H}$, $M(b\bar{e}^+)_{min}$ and $\cos\theta_{b_1b_2}^*$ for the $pp \rightarrow e^+\nu_e\mu^-\bar{\nu}_\mu b\bar{b}H$ process at the LHC with $\sqrt{s} = 13$ TeV. The upper panels show NWA and NWA_{LOdec} (dashed lines) results. The lower panels provide the ratio NWA/NWA_{LOdec} of the normalised distributions. Scale uncertainties are given for $\alpha_{CP} = 0$ in the upper panel while Monte Carlo integration errors are displayed in both panels.*

off-shell result, its contribution increases substantially from 10% for the \mathcal{CP} -even Higgs boson to 34% for the \mathcal{CP} -odd Higgs boson. Again, even at the beginning of the spectrum, the SR contribution is of the order of 16% for $\alpha_{CP} = \pi/2$, while for the SM Higgs boson case we have a rather constant contribution of the order of 10% for the whole plotted range. Consequently, the DR part is reduced from around 90% for the $\alpha_{CP} = 0$ case down to 84% for the $\alpha_{CP} = \pi/2$ one.

Finally, we investigate the effects of the inclusion of higher-order QCD corrections to top-quark decays in an NLO calculation. As an example, we display the observables p_{T,b_1} , $p_{T,H}$, $M(b\bar{e}^+)_{min}$ and $\cos\theta_{b_1b_2}^*$ in Figure 10. In each case we plot the full NWA predictions (solid lines) and the NWA_{LOdec}

ones (dashed lines). The lower panels display the ratio $\text{NWA}/\text{NWA}_{\text{LOdec}}$ of the normalised differential cross-section distributions. For p_{T,b_1} we find that the NLO QCD corrections to the top-quark decays amount to about 20% for small transverse momenta and about 10% for larger values of p_{T,b_1} . They are very similar for all three \mathcal{CP} configurations as the corresponding normalized ratios differ by less than 2% amongst themselves. For $p_{T,H}$ the shape distortions due to QCD corrections in the decay stage range from -5% to 10% for all three \mathcal{CP} configurations. Thus again, the higher-order effects do not depend on the \mathcal{CP} nature of the Higgs boson. Even for $M(be^+)_{\text{min}}$, for which we have found huge differences between the three different \mathcal{CP} states in the full off-shell calculation, the inclusion of corrections in top-quark decays is similar in all three cases. Still, we find a large enhancement of QCD corrections for $M(be^+)_{\text{min}} > 153$ GeV of the order of 30%. Even for $M(be^+)_{\text{min}} < 153$ GeV the $\mathcal{O}(\alpha_s)$ corrections to the top-quark decays lead to substantial shape changes ranging from about -20% up to $+10\%$. Therefore, in the vicinity of the kinematical edge, the overall shape distortions reach up to 50%. The dimensionless observables are less affected by higher-order effects in the top-quark decays. For angular distributions, like $\cos\theta_{b_1 b_2}^*$, the shape distortions in the normalised ratio do not exceed 4% for all three \mathcal{CP} configurations. Furthermore, these shape distortions do not differ by more than 4% amongst the different \mathcal{CP} states.

Thus, as expected and already discussed at the integrated fiducial cross-section level, the NLO QCD corrections to top-quark decays are similar in size and shape for all three considered \mathcal{CP} states of the Higgs boson in differential cross-section distributions. Accordingly, on their own they do not help in deciphering the \mathcal{CP} nature of the Higgs boson. Nevertheless, higher-order corrections to top-quark decays cannot simply be omitted. Not only do they range from a few percent up to 30% depending on the phase-space region, introducing vast distortions in the shape of various observables, but they also significantly impact the final theoretical uncertainties. Therefore, they should not be ignored in high-precision theoretical predictions for the $pp \rightarrow e^+ \nu_e \mu^- \bar{\nu}_\mu b \bar{b} H$ process.

In summary, when considering high precision theoretical predictions for the associated production of the Higgs boson and top-quark pairs various effects have to be taken into account. We have seen that NLO QCD corrections to top-quark production and decays are indispensable when studying the \mathcal{CP} property of the Higgs boson. Furthermore, the non-factorisable higher-order corrections, which introduce the cross-talk between the production and decay stage, play a crucial role. The latter cannot simply be approximated by some overall factor. Indeed, they are vastly different for various observables and their size depends on the examined phase-space region.

6 Summary

In this paper we have presented NLO QCD calculations for the $pp \rightarrow e^+ \nu_e \mu^- \bar{\nu}_\mu b \bar{b} H$ process at the LHC with $\sqrt{s} = 13$ TeV for the \mathcal{CP} -even and \mathcal{CP} -odd state of the Higgs boson as well as for possible mixing between these two states. We have placed particular emphasis on how the different \mathcal{CP} states are affected by higher-order corrections and full off-shell top-quark and W gauge boson effects. To this end, we have compared integrated fiducial cross-sections and differential distributions including full off-shell effects to those computed in the narrow-width approximation for the \mathcal{CP} -even ($\alpha_{CP} = 0$), \mathcal{CP} -odd ($\alpha_{CP} = \pi/2$) and \mathcal{CP} -mixed ($\alpha_{CP} = \pi/4$) states. For the full off-shell calculations we have taken into account all double-, single- and non-resonant diagrams as well as interference effects between those and introduced Breit-Wigner distributions for the unstable top quarks and gauge bosons through the complex-mass scheme to describe their invariant mass distributions.

As a first step, we have demonstrated that even at the level of integrated fiducial cross-sections, off-shell effects can significantly exceed the typical size of $\mathcal{O}(\Gamma/m)$. While these effects are below

one percent for the \mathcal{CP} -even and -mixed scenarios and thus still well within scale uncertainties, they reach 13% – 14% for the pseudoscalar Higgs boson. This increase for the $\alpha_{CP} = \pi/2$ case is driven by a substantially larger contribution from the single-resonant top-quark region of the phase space. In addition, we have investigated how the α_{CP} -dependence of the integrated cross-section changes between the NWA and the full off-shell treatment. Due to the absence of any HVV couplings in the NWA, the corresponding integrated cross-section is symmetric around $\alpha_{CP} = \pi/2$. However, this symmetry is broken if full off-shell effects are included. This is a result of interference effects between diagrams in which the Higgs boson is radiated of a gauge boson and those in which it is emitted from a top quark. These contributions are proportional to $\cos(\alpha_{CP})$ instead of $\cos^2(\alpha_{CP})$ or $\sin^2(\alpha_{CP})$ and thus not symmetric around $\alpha_{CP} = \pi/2$. Consequently, the integrated fiducial cross-section is about 7% larger for $\alpha_{CP} = \pi$ than for the SM case.

Just like the off-shell effects, NLO corrections are also largest for the \mathcal{CP} -odd scenario. We have shown that the \mathcal{K} -factor is of the order of 1.21 – 1.23 for the SM and \mathcal{CP} -mixed cases and 1.31 for the \mathcal{CP} -odd one. Furthermore, theoretical scale uncertainties are substantially reduced when higher-order effects are incorporated. Specifically, they are at the level of 31% – 34% at LO and in the range of 5% – 6% for the NLO predictions. When only considering NLO QCD corrections to the production stage, we have observed that the size of higher-order effects increases together with the corresponding scale uncertainties. Indeed, not only the \mathcal{K} -factor is now in the range of 1.27 – 1.28 for the \mathcal{CP} -even and \mathcal{CP} -mixed Higgs boson and up to $\mathcal{K} = 1.34$ for the \mathcal{CP} -odd case, but also theoretical uncertainties due to the scale dependence increase up to 11%. Therefore, they are almost twice as large as in the full NWA or when full off-shell effects are included. Independently of the modeling, the scale dependence is roughly the same when comparing the different Higgs boson \mathcal{CP} states.

Next to the overall normalisation, the NLO QCD corrections also change the shape of several differential cross-section distributions. In contrast to their effects on the normalisation at the fiducial cross-section level, the shape distortions are generally larger for the SM case. This is particularly apparent in the case of the $p_{T,\text{miss}}$ and $M(be^+)_{\text{min}}$ distributions. For these observables the smaller shape distortions for the pseudoscalar Higgs boson can mainly be ascribed to the generally harder Higgs boson radiation and the larger relative size of single- and non-resonant contributions. In general, the \mathcal{K} -factors are larger in the high- p_T and -mass regions, irrespective of the Higgs bosons \mathcal{CP} state. Just like in the case of $t\bar{t}$ production and for other $t\bar{t}$ -associated production processes, NLO QCD corrections are especially large for the $M(be^+)_{\text{min}}$ observable above the kinematical edge around 153 GeV. In this phase-space region higher-order effects can even exceed 100% in the \mathcal{CP} -even and \mathcal{CP} -mixed cases.

In the second part of our discussion on differential cross-section distributions we have investigated the impact of full off-shell effects on the distribution shapes. Just as for the integrated fiducial cross-section, the effects are fairly small for the SM and \mathcal{CP} -mixed cases apart from the high- $M(be^+)_{\text{min}}$ and $-M_{T2,t}$ regions. Both of these observables have kinematical edges which are related to the masses of unstable intermediate particles. For these two observables full off-shell effects can exceed 50% above these edges. For the pseudoscalar Higgs boson, on the other hand, all observables are significantly affected by off-shell effects. Again, these effects are largest for $M(be^+)_{\text{min}}$ and $M_{T2,t}$ at up to 90%. However, even in observables without kinematic edges the differences can reach 45% in dimensionful and 20% in dimensionless observables. In general, the full off-shell effects are larger in the high- p_T and -mass phase-space regions and for small angles between the decay products coming from two different top quarks.

These changes in the behaviour of differential distributions also have a significant impact on how well one can distinguish the three Higgs boson \mathcal{CP} states from each other at the differential

fiducial cross-section level. We have shown that while the normalised distributions for the \mathcal{CP} -even and \mathcal{CP} -mixed cases are generally quite similar to each other, the \mathcal{CP} -odd case leads to much more pronounced distribution tails in transverse momentum and invariant mass distributions. Again, this is mostly a result of the harder radiation of a pseudoscalar Higgs boson compared to a scalar one. For $M_{T2,t}$ this effect is so large that the \mathcal{CP} -odd distribution actually exceeds the one for the SM case above 240 GeV even though the integrated cross-section is about five times as large for the latter. Although not quite as drastic, the shape differences in H_T , $p_{T,H}$ and $M(be^+)_{\min}$ still result in ratios of normalised distributions that reach a factor 2 or more in the tails of the respective distributions. Amongst dimensionless cross-section distributions we have found that the $\cos\theta_{e^+\mu^-}^*$ observable is the most promising candidate for distinguishing the different \mathcal{CP} states of the Higgs boson.

In addition, we have discussed the effects of omitting NLO QCD corrections in top-quark decays at the differential fiducial cross-section level by comparing the full NWA with the NWA_{LOdec} predictions. In contrast to the full NLO QCD corrections, the shape distortions coming from NLO QCD corrections to top-quark decays are largely independent of the \mathcal{CP} state, even above kinematic edges. Nevertheless, they should be taken into account as they can reach up to 30% depending on the considered observable and phase-space region. Furthermore, they introduce vast shape distortions and significantly impact the size of scale uncertainties.

In summary, both NLO QCD corrections and full off-shell effects of the top quark and W gauge boson have a significant impact on the normalisation and shape of various differential cross-section distributions for the $pp \rightarrow e^+\nu_e\mu^-\bar{\nu}_\mu b\bar{b}H$ process at the LHC with $\sqrt{s} = 13$ TeV for all three Higgs boson \mathcal{CP} states. However, the most affected is the \mathcal{CP} -odd Higgs boson. For the \mathcal{CP} -even and -mixed cases higher-order corrections play a crucial role but full off-shell effects come into play mostly in the case of observables with kinematic edges such as $M(be^+)_{\min}$ and $M_{T2,t}$. Due to these kinematic edges, these observables are also the ones that are most sensitive to the \mathcal{CP} state of the Higgs boson.

Finally, let us mention again that the calculations presented in this paper and the HELAC-NLO framework constructed for this work could easily be altered in order to obtain results for a general beyond the SM Higgs-boson sector and are thus not limited to predictions for an SM-like Higgs boson.

Acknowledgments

The work was supported by the Deutsche Forschungsgemeinschaft (DFG) under grant 396021762 – TRR 257: *P3H - Particle Physics Phenomenology after the Higgs Discovery* and by the DFG under grant 400140256 - GRK 2497: *The physics of the heaviest particles at the LHC*.

Support by a grant of the Bundesministerium für Bildung und Forschung (BMBF) is additionally acknowledged.

The authors gratefully acknowledge the computing time granted by the Resource Allocation Board and provided on the supercomputer CLAIX at RWTH Aachen University as part of the NHR infrastructure. The calculations for this research were conducted with computing resources under the projects `rwth0414` and `rwth0871`.

References

- [1] ATLAS collaboration, *Observation of a new particle in the search for the Standard Model Higgs boson with the ATLAS detector at the LHC*, *Phys. Lett. B* **716** (2012) 1 [[1207.7214](#)].
- [2] CMS collaboration, *Observation of a New Boson at a Mass of 125 GeV with the CMS Experiment at the LHC*, *Phys. Lett. B* **716** (2012) 30 [[1207.7235](#)].

- [3] CMS collaboration, *Constraints on the spin-parity and anomalous HVV couplings of the Higgs boson in proton collisions at 7 and 8 TeV*, *Phys. Rev. D* **92** (2015) 012004 [[1411.3441](#)].
- [4] ATLAS collaboration, *Study of the spin and parity of the Higgs boson in diboson decays with the ATLAS detector*, *Eur. Phys. J. C* **75** (2015) 476 [[1506.05669](#)].
- [5] ATLAS collaboration, *Test of CP Invariance in vector-boson fusion production of the Higgs boson using the Optimal Observable method in the ditau decay channel with the ATLAS detector*, *Eur. Phys. J. C* **76** (2016) 658 [[1602.04516](#)].
- [6] CMS collaboration, *Constraints on anomalous Higgs boson couplings using production and decay information in the four-lepton final state*, *Phys. Lett. B* **775** (2017) 1 [[1707.00541](#)].
- [7] CMS collaboration, *Measurements of the Higgs boson width and anomalous HVV couplings from on-shell and off-shell production in the four-lepton final state*, *Phys. Rev. D* **99** (2019) 112003 [[1901.00174](#)].
- [8] CMS collaboration, *Constraints on anomalous HVV couplings from the production of Higgs bosons decaying to τ lepton pairs*, *Phys. Rev. D* **100** (2019) 112002 [[1903.06973](#)].
- [9] ATLAS collaboration, *Test of CP invariance in vector-boson fusion production of the Higgs boson in the $H \rightarrow \tau^+\tau^-$ channel in pp collisions at $\sqrt{s} = 13$ TeV with the ATLAS detector*, *Phys. Lett. B* **805** (2020) 135426 [[2002.05315](#)].
- [10] CMS collaboration, *Constraints on anomalous Higgs boson couplings to vector bosons and fermions in its production and decay using the four-lepton final state*, *Phys. Rev. D* **104** (2021) 052004 [[2104.12152](#)].
- [11] ATLAS collaboration, *Measurements of Higgs boson production heis and couplings in diboson final states with the ATLAS detector at the LHC*, *Phys. Lett. B* **726** (2013) 88 [[1307.1427](#)].
- [12] CMS collaboration, *Precise determination of the mass of the Higgs boson and tests of compatibility of its couplings with the standard model predictions using proton collisions at 7 and 8 TeV*, *Eur. Phys. J. C* **75** (2015) 212 [[1412.8662](#)].
- [13] ATLAS, CMS collaboration, *Measurements of the Higgs boson production and decay rates and constraints on its couplings from a combined ATLAS and CMS analysis of the LHC pp collision data at $\sqrt{s} = 7$ and 8 TeV*, *JHEP* **08** (2016) 045 [[1606.02266](#)].
- [14] A. D. Sakharov, *Violation of cp invariance, c asymmetry, and baryon asymmetry of the universe*, *Soviet Physics Uspekhi* **34** (1991) 392.
- [15] V. A. Kuzmin, V. A. Rubakov and M. E. Shaposhnikov, *On the Anomalous Electroweak Baryon Number Nonconservation in the Early Universe*, *Phys. Lett. B* **155** (1985) 36.
- [16] J. F. Gunion, H. E. Haber, G. L. Kane and S. Dawson, *The Higgs Hunter's Guide*, vol. 80. 2000.
- [17] J. F. Gunion and H. E. Haber, *The CP conserving two Higgs doublet model: The Approach to the decoupling limit*, *Phys. Rev. D* **67** (2003) 075019 [[hep-ph/0207010](#)].
- [18] G. C. Branco, P. M. Ferreira, L. Lavoura, M. N. Rebelo, M. Sher and J. P. Silva, *Theory and phenomenology of two-Higgs-doublet models*, *Phys. Rept.* **516** (2012) 1 [[1106.0034](#)].
- [19] B. Grzadkowski, O. M. Ogreid and P. Osland, *Measuring CP violation in Two-Higgs-Doublet models in light of the LHC Higgs data*, *JHEP* **11** (2014) 084 [[1409.7265](#)].
- [20] J. Ellis, D. S. Hwang, K. Sakurai and M. Takeuchi, *Disentangling Higgs-Top Couplings in Associated Production*, *JHEP* **04** (2014) 004 [[1312.5736](#)].
- [21] F. Boudjema, R. M. Godbole, D. Guadagnoli and K. A. Mohan, *Lab-frame observables for probing the top-Higgs interaction*, *Phys. Rev. D* **92** (2015) 015019 [[1501.03157](#)].
- [22] M. R. Buckley and D. Goncalves, *Boosting the Direct CP Measurement of the Higgs-Top Coupling*, *Phys. Rev. Lett.* **116** (2016) 091801 [[1507.07926](#)].

- [23] S. Amor Dos Santos et al., *Probing the CP nature of the Higgs coupling in $t\bar{t}h$ events at the LHC*, *Phys. Rev. D* **96** (2017) 013004 [[1704.03565](#)].
- [24] CMS collaboration, *Measurements of properties of the Higgs boson decaying into the four-lepton final state in pp collisions at $\sqrt{s} = 13$ TeV*, *JHEP* **11** (2017) 047 [[1706.09936](#)].
- [25] CMS collaboration, *Measurements of Higgs boson properties in the diphoton decay channel in proton-proton collisions at $\sqrt{s} = 13$ TeV*, *JHEP* **11** (2018) 185 [[1804.02716](#)].
- [26] ATLAS collaboration, *Combined measurements of Higgs boson production and decay using up to 80 fb^{-1} of proton-proton collision data at $\sqrt{s} = 13$ TeV collected with the ATLAS experiment*, [ATLAS-CONF-2018-031], .
- [27] CMS collaboration, *Combined measurements of Higgs boson couplings in proton-proton collisions at $\sqrt{s} = 13$ TeV*, *Eur. Phys. J. C* **79** (2019) 421 [[1809.10733](#)].
- [28] ATLAS collaboration, *Observation of Higgs boson production in association with a top quark pair at the LHC with the ATLAS detector*, *Phys. Lett. B* **784** (2018) 173 [[1806.00425](#)].
- [29] CMS collaboration, *Observation of $t\bar{t}H$ production*, *Phys. Rev. Lett.* **120** (2018) 231801 [[1804.02610](#)].
- [30] ATLAS collaboration, *CP Properties of Higgs Boson Interactions with Top Quarks in the $t\bar{t}H$ and tH Processes Using $H \rightarrow \gamma\gamma$ with the ATLAS Detector*, *Phys. Rev. Lett.* **125** (2020) 061802 [[2004.04545](#)].
- [31] CMS collaboration, *Measurements of $t\bar{t}H$ Production and the CP Structure of the Yukawa Interaction between the Higgs Boson and Top Quark in the Diphoton Decay Channel*, *Phys. Rev. Lett.* **125** (2020) 061801 [[2003.10866](#)].
- [32] CMS collaboration, *Search for CP violation in $t\bar{t}H$ and tH production in multilepton channels at $\sqrt{s} = 13$ TeV*, [CMS-PAS-HIG-21-006], .
- [33] CMS collaboration, *Analysis of the CP structure of the Yukawa coupling between the Higgs boson and τ leptons in proton-proton collisions at $\sqrt{s} = 13$ TeV*, [CMS-PAS-HIG-20-006], tech. rep., CERN, Geneva, 2020.
- [34] P. Artoisenet et al., *A framework for Higgs characterisation*, *JHEP* **11** (2013) 043 [[1306.6464](#)].
- [35] W.-S. Hou, M. Kohda and T. Modak, *Probing for extra top Yukawa couplings in light of $t\bar{t}h(125)$ observation*, *Phys. Rev. D* **98** (2018) 075007 [[1806.06018](#)].
- [36] H. Bahl, P. Bechtle, S. Heinemeyer, J. Katzy, T. Klingl, K. Peters et al., *Indirect CP probes of the Higgs-top-quark interaction: current LHC constraints and future opportunities*, *JHEP* **11** (2020) 127 [[2007.08542](#)].
- [37] D. Azevedo, R. Capucha, E. Gouveia, A. Onofre and R. Santos, *Light Higgs searches in $t\bar{t}\phi$ production at the LHC*, *JHEP* **04** (2021) 077 [[2012.10730](#)].
- [38] B. Bortolato, J. F. Kamenik, N. Košnik and A. Smolkovič, *Optimized probes of CP -odd effects in the $t\bar{t}h$ process at hadron colliders*, *Nucl. Phys. B* **964** (2021) 115328 [[2006.13110](#)].
- [39] T. Martini, R.-Q. Pan, M. Schulze and M. Xiao, *Probing the CP structure of the top quark Yukawa coupling: Loop sensitivity versus on-shell sensitivity*, *Phys. Rev. D* **104** (2021) 055045 [[2104.04277](#)].
- [40] H. Bahl and S. Brass, *Constraining CP-violation in the Higgs-top-quark interaction using machine-learning-based inference*, *JHEP* **03** (2022) 017 [[2110.10177](#)].
- [41] R. Frederix, S. Frixione, V. Hirschi, F. Maltoni, R. Pittau and P. Torrielli, *Scalar and pseudoscalar Higgs production in association with a top-antitop pair*, *Phys. Lett. B* **701** (2011) 427 [[1104.5613](#)].
- [42] M. V. Garzelli, A. Kardos, C. G. Papadopoulos and Z. Trocsanyi, *Standard Model Higgs boson production in association with a top anti-top pair at NLO with parton showering*, *EPL* **96** (2011) 11001 [[1108.0387](#)].

- [43] P. Artoisenet, R. Frederix, O. Mattelaer and R. Rietkerk, *Automatic spin-entangled decays of heavy resonances in Monte Carlo simulations*, *JHEP* **03** (2013) 015 [[1212.3460](#)].
- [44] S. Biswas, R. Frederix, E. Gabrielli and B. Mele, *Enhancing the $t\bar{t}H$ signal through top-quark spin polarization effects at the LHC*, *JHEP* **07** (2014) 020 [[1403.1790](#)].
- [45] F. Demartin, F. Maltoni, K. Mawatari, B. Page and M. Zaro, *Higgs characterisation at NLO in QCD: CP properties of the top-quark Yukawa interaction*, *Eur. Phys. J. C* **74** (2014) 3065 [[1407.5089](#)].
- [46] H. B. Hartanto, B. Jager, L. Reina and D. Wackerroth, *Higgs boson production in association with top quarks in the POWHEG BOX*, *Phys. Rev. D* **91** (2015) 094003 [[1501.04498](#)].
- [47] F. Demartin, F. Maltoni, K. Mawatari and M. Zaro, *Higgs production in association with a single top quark at the LHC*, *Eur. Phys. J. C* **75** (2015) 267 [[1504.00611](#)].
- [48] F. Demartin, B. Maier, F. Maltoni, K. Mawatari and M. Zaro, *tWH associated production at the LHC*, *Eur. Phys. J. C* **77** (2017) 34 [[1607.05862](#)].
- [49] S. Frixione, E. Laenen, P. Motylinski, B. R. Webber and C. D. White, *Single-top hadroproduction in association with a W boson*, *JHEP* **07** (2008) 029 [[0805.3067](#)].
- [50] T. Jezo, J. M. Lindert, P. Nason, C. Oleari and S. Pozzorini, *An NLO+PS generator for $t\bar{t}$ and Wt production and decay including non-resonant and interference effects*, *Eur. Phys. J. C* **76** (2016) no.12, 691 [[1607.04538](#)].
- [51] A. Denner and R. Feger, *NLO QCD corrections to off-shell top-antitop production with leptonic decays in association with a Higgs boson at the LHC*, *JHEP* **11** (2015) 209 [[1506.07448](#)].
- [52] D. Stremmer and M. Worek, *Production and decay of the Higgs boson in association with top quarks*, *JHEP* **02** (2022) 196 [[2111.01427](#)].
- [53] A. Denner, J.-N. Lang, M. Pellen and S. Uccirati, *Higgs production in association with off-shell top-antitop pairs at NLO EW and QCD at the LHC*, *JHEP* **02** (2017) 053 [[1612.07138](#)].
- [54] R. V. Harlander, S. Y. Klein and M. Lipp, *FeynGame*, *Comput. Phys. Commun.* **256** (2020) 107465 [[2003.00896](#)].
- [55] A. Denner, S. Dittmaier, M. Roth and D. Wackerroth, *Predictions for all processes $e^+e^- \rightarrow 4$ fermions + γ* , *Nucl. Phys. B* **560** (1999) 33 [[hep-ph/9904472](#)].
- [56] A. Denner, S. Dittmaier, M. Roth and L. H. Wieders, *Electroweak corrections to charged-current $e^+e^- \rightarrow 4$ fermion processes: Technical details and further results*, *Nucl. Phys. B* **724** (2005) 247 [[hep-ph/0505042](#)].
- [57] G. Bevilacqua, M. Czakon, A. van Hameren, C. G. Papadopoulos and M. Worek, *Complete off-shell effects in top quark pair hadroproduction with leptonic decay at next-to-leading order*, *JHEP* **02** (2011) 083 [[1012.4230](#)].
- [58] A. Denner, S. Dittmaier, S. Kallweit and S. Pozzorini, *NLO QCD corrections to off-shell top-antitop production with leptonic decays at hadron colliders*, *JHEP* **10** (2012) 110 [[1207.5018](#)].
- [59] G. Bevilacqua, M. Czakon, M. V. Garzelli, A. van Hameren, A. Kardos, C. G. Papadopoulos et al., *HELAC-NLO*, *Comput. Phys. Commun.* **184** (2013) 986 [[1110.1499](#)].
- [60] G. Bevilacqua, H. B. Hartanto, M. Kraus, T. Weber and M. Worek, *Off-shell vs on-shell modelling of top quarks in photon associated production*, *JHEP* **03** (2020) 154 [[1912.09999](#)].
- [61] M. Czakon, C. G. Papadopoulos and M. Worek, *Polarizing the Dipoles*, *JHEP* **08** (2009) 085 [[0905.0883](#)].
- [62] A. van Hameren, C. G. Papadopoulos and R. Pittau, *Automated one-loop calculations: A Proof of concept*, *JHEP* **09** (2009) 106 [[0903.4665](#)].

- [63] P. Draggiotis, R. H. P. Kleiss and C. G. Papadopoulos, *On the computation of multigluon amplitudes*, *Phys. Lett. B* **439** (1998) 157 [[hep-ph/9807207](#)].
- [64] P. D. Draggiotis, R. H. P. Kleiss and C. G. Papadopoulos, *Multijet production in hadron collisions*, *Eur. Phys. J. C* **24** (2002) 447 [[hep-ph/0202201](#)].
- [65] C. G. Papadopoulos and M. Worek, *Multi-parton cross sections at hadron colliders*, *Eur. Phys. J. C* **50** (2007) 843 [[hep-ph/0512150](#)].
- [66] A. van Hameren, *PARNI for importance sampling and density estimation*, *Acta Phys. Polon. B* **40** (2009) 259 [[0710.2448](#)].
- [67] A. van Hameren, *Kaleu: A General-Purpose Parton-Level Phase Space Generator*, [1003.4953](#).
- [68] G. Bevilacqua, H. B. Hartanto, M. Kraus, T. Weber and M. Worek, *Hard Photons in Hadroproduction of Top Quarks with Realistic Final States*, *JHEP* **10** (2018) 158 [[1803.09916](#)].
- [69] G. Bevilacqua, H. B. Hartanto, M. Kraus, T. Weber and M. Worek, *Towards constraining Dark Matter at the LHC: Higher order QCD predictions for $t\bar{t} + Z(Z \rightarrow \nu_\ell \bar{\nu}_\ell)$* , *JHEP* **11** (2019) 001 [[1907.09359](#)].
- [70] G. Bevilacqua, H.-Y. Bi, H. B. Hartanto, M. Kraus and M. Worek, *The simplest of them all: $t\bar{t}W^\pm$ at NLO accuracy in QCD*, *JHEP* **08** (2020) 043 [[2005.09427](#)].
- [71] G. Ossola, C. G. Papadopoulos and R. Pittau, *CutTools: A Program implementing the OPP reduction method to compute one-loop amplitudes*, *JHEP* **03** (2008) 042 [[0711.3596](#)].
- [72] G. Ossola, C. G. Papadopoulos and R. Pittau, *Reducing full one-loop amplitudes to scalar integrals at the integrand level*, *Nucl. Phys. B* **763** (2007) 147 [[hep-ph/0609007](#)].
- [73] A. van Hameren, *OneLOop: For the evaluation of one-loop scalar functions*, *Comput. Phys. Commun.* **182** (2011) 2427 [[1007.4716](#)].
- [74] S. Catani and M. H. Seymour, *A General algorithm for calculating jet cross-sections in NLO QCD*, *Nucl. Phys. B* **485** (1997) 291 [[hep-ph/9605323](#)].
- [75] S. Catani, S. Dittmaier, M. H. Seymour and Z. Trocsanyi, *The Dipole formalism for next-to-leading order QCD calculations with massive partons*, *Nucl. Phys. B* **627** (2002) 189 [[hep-ph/0201036](#)].
- [76] G. Bevilacqua, M. Czakon, M. Kubocz and M. Worek, *Complete Nagy-Soper subtraction for next-to-leading order calculations in QCD*, *JHEP* **10** (2013) 204 [[1308.5605](#)].
- [77] J. M. Campbell, R. K. Ellis and F. Tramontano, *Single top production and decay at next-to-leading order*, *Phys. Rev. D* **70** (2004) 094012 [[hep-ph/0408158](#)].
- [78] G. Bevilacqua, H. B. Hartanto, M. Kraus and M. Worek, *Off-shell Top Quarks with One Jet at the LHC: A comprehensive analysis at NLO QCD*, *JHEP* **11** (2016) 098 [[1609.01659](#)].
- [79] J. Alwall et al., *A Standard format for Les Houches event files*, *Comput. Phys. Commun.* **176** (2007) 300 [[hep-ph/0609017](#)].
- [80] I. Antcheva et al., *ROOT: A C++ framework for petabyte data storage, statistical analysis and visualization*, *Comput. Phys. Commun.* **180** (2009) 2499 [[1508.07749](#)].
- [81] J. Alwall, R. Frederix, S. Frixione, V. Hirschi, F. Maltoni, O. Mattelaer et al., *The automated computation of tree-level and next-to-leading order differential cross sections, and their matching to parton shower simulations*, *JHEP* **07** (2014) 079 [[1405.0301](#)].
- [82] V. Hirschi, R. Frederix, S. Frixione, M. V. Garzelli, F. Maltoni and R. Pittau, *Automation of one-loop QCD corrections*, *JHEP* **05** (2011) 044 [[1103.0621](#)].
- [83] R. Kleiss, W. J. Stirling and S. D. Ellis, *A New Monte Carlo Treatment of Multiparticle Phase Space at High-energies*, *Comput. Phys. Commun.* **40** (1986) 359.
- [84] Z. Nagy and Z. Trocsanyi, *Next-to-leading order calculation of four jet observables in electron positron annihilation*, *Phys. Rev. D* **59** (1999) 014020 [[hep-ph/9806317](#)].

- [85] Z. Nagy, *Next-to-leading order calculation of three jet observables in hadron hadron collision*, *Phys. Rev. D* **68** (2003) 094002 [[hep-ph/0307268](#)].
- [86] G. Bevilacqua, M. Czakon, C. G. Papadopoulos, R. Pittau and M. Worek, *Assault on the NLO Wishlist: $pp \rightarrow t\bar{t}b\bar{b}$* , *JHEP* **09** (2009) 109 [[0907.4723](#)].
- [87] M. Czakon, H. B. Hartanto, M. Kraus and M. Worek, *Matching the Nagy-Soper parton shower at next-to-leading order*, *JHEP* **06** (2015) 033 [[1502.00925](#)].
- [88] A. Buckley, J. Ferrando, S. Lloyd, K. Nordström, B. Page, M. Rüfenacht et al., *LHAPDF6: parton density access in the LHC precision era*, *Eur. Phys. J. C* **75** (2015) 132 [[1412.7420](#)].
- [89] NNPDF collaboration, *Parton distributions from high-precision collider data*, *Eur. Phys. J. C* **77** (2017) 663 [[1706.00428](#)].
- [90] M. Jezabek and J. H. Kuhn, *QCD Corrections to Semileptonic Decays of Heavy Quarks*, *Nucl. Phys. B* **314** (1989) 1.
- [91] M. Cacciari, G. P. Salam and G. Soyez, *The anti- k_t jet clustering algorithm*, *JHEP* **04** (2008) 063 [[0802.1189](#)].
- [92] ATLAS collaboration, *Measurements of gluon fusion and vector-boson-fusion production of the Higgs boson in $H \rightarrow WW^* \rightarrow e\nu\mu\nu$ decays using pp collisions at $\sqrt{s} = 13$ TeV with the ATLAS detector*, [ATLAS-CONF-2021-014], tech. rep., CERN, Geneva, Mar, 2021.
- [93] CMS collaboration, *Measurements of Higgs boson production via gluon fusion and vector boson fusion in the diphoton decay channel at $\sqrt{s} = 13$ TeV*, [CMS-PAS-HIG-18-029], tech. rep., CERN, Geneva, 2019.
- [94] M. Aoki, S. Kanemura, K. Tsumura and K. Yagyu, *Models of Yukawa interaction in the two Higgs doublet model, and their collider phenomenology*, *Phys. Rev. D* **80** (2009) 015017 [[0902.4665](#)].
- [95] T. Plehn, D. L. Rainwater and D. Zeppenfeld, *Determining the Structure of Higgs Couplings at the LHC*, *Phys. Rev. Lett.* **88** (2002), 051801 [[hep-ph/0105325](#)].
- [96] U. Haisch, P. Pani and G. Polesello, *Determining the CP nature of spin-0 mediators in associated production of dark matter and $t\bar{t}$ pairs*, *JHEP* **02** (2017) 131 [[1611.09841](#)].
- [97] S. Dittmaier, M. Kramer, Y. Liao, M. Spira and P. M. Zerwas, *Higgs radiation off quarks in supersymmetric theories at e^+e^- colliders*, *Phys. Lett. B* **478** (2000) 247 [[hep-ph/0002035](#)].
- [98] S. Dawson and L. Reina, *QCD corrections to associated Higgs boson production*, *Phys. Rev. D* **57** (1998) 5851 [[hep-ph/9712400](#)].
- [99] V. S. Fadin, V. A. Khoze and A. D. Martin, *How suppressed are the radiative interference effects in heavy instable particle production?*, *Phys. Lett. B* **320** (1994) 141 [[hep-ph/9309234](#)].
- [100] J. Hermann and M. Worek, *The impact of top-quark modelling on the exclusion limits in $t\bar{t} + DM$ searches at the LHC*, *Eur. Phys. J. C* **81** (2021) 1029 [[2108.01089](#)].
- [101] G. Bevilacqua, H. B. Hartanto, M. Kraus, J. Nasufi and M. Worek, *NLO QCD corrections to full off-shell production of $t\bar{t}Z$ including leptonic decays*, *JHEP* **08** (2022) 060 [[2203.15688](#)].
- [102] M. Czakon, A. Mitov and R. Poncelet, *NNLO QCD corrections to leptonic observables in top-quark pair production and decay*, *JHEP* **05** (2021) 212 [[2008.11133](#)].
- [103] A. J. Barr, *Measuring slepton spin at the LHC*, *JHEP* **02** (2006) 042 [[hep-ph/0511115](#)].
- [104] A. Barr, C. Lester and P. Stephens, *$m(T_2)$: The Truth behind the glamour*, *J. Phys. G* **29** (2003) 2343 [[hep-ph/0304226](#)].
- [105] C. G. Lester and D. J. Summers, *Measuring masses of semiinvisibly decaying particles pair produced at hadron colliders*, *Phys. Lett. B* **463** (1999) 99 [[hep-ph/9906349](#)].
- [106] C. G. Lester and B. Nachman, *Bisection-based asymmetric M_{T_2} computation: a higher precision calculator than existing symmetric methods*, *JHEP* **03** (2015) 100 [[1411.4312](#)].

- [107] N. Kauer and D. Zeppenfeld, *Finite width effects in top quark production at hadron colliders*, *Phys. Rev. D* **65** (2002) 014021 [[hep-ph/0107181](#)].
- [108] S. Liebler, G. Moortgat-Pick and A. S. Papanastasiou, *Probing the top-quark width through ratios of resonance contributions of $e^+e^- \rightarrow W^+W^-b\bar{b}$* , *JHEP* **03** (2016) 099 [[1511.02350](#)].
- [109] A. Baskakov, E. Boos and L. Dudko, *Model independent top quark width measurement using a combination of resonant and nonresonant cross sections*, *Phys. Rev. D* **98** (2018) no.11, 116011 [[1807.11193](#)].
- [110] G. Bevilacqua, H. Y. Bi, H. B. Hartanto, M. Kraus, J. Nasufi and M. Worek, *NLO QCD corrections to off-shell $t\bar{t}W^\pm$ production at the LHC: correlations and asymmetries*, *Eur. Phys. J. C* **81** (2021) no.7, 675 [[2012.01363](#)].